


Performance enhancement of quantum Brayton engine via Bose-Einstein condensationHuilin Ruan,¹ Jiehong Yuan,¹ Yang Xu,¹ Jizhou He,¹ Yongli Ma^{2,*} and Jianhui Wang^{1,2,†}¹*Department of Physics, Nanchang University, Nanchang 330031, China*²*State Key Laboratory of Surface Physics and Department of Physics, Fudan University, Shanghai 200433, China* (Received 13 October 2023; revised 30 December 2023; accepted 1 February 2024; published 23 February 2024)

Bose-Einstein condensation is a quintessential characteristic of Bose systems. We investigate the finite-time performance of an endoreversible quantum Brayton heat engine operating with an ideal Bose gas with a finite number of particles confined in a d -dimensional harmonic trap. The working medium of these engines may work in the condensation, noncondensation, and near-critical point regimes, respectively. We demonstrate that the existence of the phase transition during the cycle leads to enhanced engine performance by increasing power output and efficiencies corresponding to maximum power and maximum efficient power. We also show that the quantum engine working across the Bose-Einstein condensation in N -particle Bose gas outperforms an ensemble of independent single-particle heat engines. The difference in the machine performance can be explained in terms of the behavior of specific heat at constant pressure near the critical point regime.

DOI: [10.1103/PhysRevE.109.024126](https://doi.org/10.1103/PhysRevE.109.024126)**I. INTRODUCTION**

Cyclic quantum heat engines [1–12], as quantum mechanical versions of the classical heat engines, can be classified into various paradigmatic models, including Carnot cycle [3,13,14], Otto cycle [5–7,10,12,15–18], Brayton cycle [19–21], and Stirling cycle [1,22,23]. These engine cycles are usually composed of different thermodynamic strokes such as adiabatic, isothermal, isochoric, and isobaric strokes. Unlike in the classical engines where the working medium is composed of classical systems, in the quantum heat engines the quantum systems are employed as the working substance. The effects induced by many particles and the quantumness in the working substance, such as the divergence of energy fluctuations at the phase transition [24–27], many-body localization [28–30], and nonclassical correlations [31–33] between particles, were observed to be advantageous for the quantum heat engines.

If the machine performance, usually associated with the efficiency and power output, is required to be improved, one route towards this improvement is to increase the specific heat of the working substance [17]. The crucial question naturally arising here is how the phase transition affects the machine performance [29,34]; the singular behaviors of the specific heat [35–37] associated with the phase transition account for a marked difference in work and heat. Recently reported cases of improved performances in quantum Otto engines [17,24] near the phase transition can, in fact, be interpreted in terms of increased specific heat.

Cooling down a gas of bosonic atoms to a very low temperature, at which the particles' separation is comparable to a thermal de Broglie wavelength, creates Bose-Einstein con-

densation [38,39] of purely quantum origin, with emphasis on the finite number of the trapped bosons [40–42]. One can focus on the Bose-Einstein condensation by considering the noninteracting Bose gas [40,41,43,44]. In the quantum domain, this state of matter should be substantially affecting the performance measures, including power output and efficiency, as suggested by recent works on quantum Otto engines [24] operating with an ideal Bose gas confined in a three-dimensional harmonic trap. Since quantum heat engines are captured by both the operation mode and quantum nature inherent in the working substance, various engine models based on different working systems in finite time have been investigated [3,22,45,46]. In addition to quantum Otto engines in which the system Hamiltonian is kept constant to realize heat exchange, a quantum Brayton engine may be another interesting engine model where the external control parameter is tuned during a cooling or heating process. Furthermore, unlike in quantum Otto refrigerators where heat exchange is associated with specific heat at constant volume, in quantum heat engines the heat is related to the specific heat at constant pressure. The two specific heats are different from each other, particularly in the phase-transition regime [47–49].

According to the second law of thermodynamics, all heat engines working between a hot and a cold reservoir of constant temperatures T_h and $T_l (< T_h)$ must not be more efficient than a Carnot engine with the efficiency $\eta_C = 1 - T_l/T_h$. The Carnot engine produces vanishing power and is of no practical application. The heat engines should speed up to operate at finite power, and thus both power output P and efficiency η are two important performance measures for the heat engines in finite time. The machine performance were always considered within the context of finite-time thermodynamics, beginning with the seminar work by Curzon and Ahlborn (CA) [50]. The efficiency at maximum power for many heat engines was found to follow some kind of universal bounds, such as the universality up to the second order of η_C (in the linear

*ylma@fudan.edu.cn

†wangjianhui@ncu.edu.cn

response regime), $\eta_C + \eta_C^2/8$, shared by the CA efficiency [51–57]. However, the efficiency at maximum power may not satisfy such bounds for some heat engines. A typical example is that the machine efficiency may approach Carnot value at finite power near the phase-transition point [17] and even at maximum power in a case with shortcut to adiabaticity [58]. In addition to the power output, the efficient power, which is defined as $\Theta \equiv P\eta$ [59–61], can be used as an optimization criterion by paying attention to both power and efficiency.

In this paper, we explore quantum Brayton engines working with an ideal Bose with a finite number of particles confined in a d -dimensional harmonic trap, within the framework of endoreversible thermodynamics. We consider the machine performance in three different regimes of operation: (i) a full condensation regime, (ii) a noncondensation regime, and (iii) a near-critical point regime. When working in the condensation regime, the engine produces relatively small work as compared to the machine operating in both noncondensation and near-critical point regimes. We show that the cycle operation at the near-critical point regime has several advantages that range from greater power output to improving efficiency. In such a case, the efficiency at maximum power for the engine working across the regime significantly surpasses the CA efficiency. We find that the thermal machine driving across the Bose-Einstein condensation in an N -particle Bose system outperforms an ensemble of independent single-particle engines. We also show that the efficiency under maximal efficient power can be significantly improved by the phase transition, recovering the known classical results under the high-temperature limit. We demonstrate that these results can be well explained in terms of specific heat at constant pressure.

II. QUANTUM BRAYTON HEAT ENGINE

A. Thermodynamics for an ideal Bose gas with a finite number of particles

We consider an ideal Bose gas with a finite number of particles confined in a d -dimensional harmonic trap. The geometric mean of the oscillator frequencies can be written in terms of the frequency of the i th axis ω_i : $\Omega = (\prod_{i=1}^d \omega_i)^{1/d}$. Within the grand-canonical-ensemble treatment, particle number N , internal energy U , and “harmonic pressure” \mathcal{P} [62] for the ideal Bose gas with temperature T can be obtained as ($\hbar \equiv k_B \equiv 1$) [63]

$$N = N_0 + \left(\frac{T}{\Omega}\right)^d g_d(z) + \lambda \Gamma(d-1) \left(\frac{T}{\Omega}\right)^{d-1} g_{d-1}(z), \quad (1)$$

$$U = Td \left(\frac{T}{\Omega}\right)^d g_{d+1}(z) + \lambda \Gamma(d) T \left(\frac{T}{\Omega}\right)^{d-1} g_d(z), \quad (2)$$

$$\mathcal{P} = T^{d+1} g_{d+1}(z) + \lambda \frac{\Gamma(d)}{d} \Omega T^d g_d(z), \quad (3)$$

where $N_0 = z/(1-z)$ is the ground-state occupation number, $z = \exp[(\mu - \varepsilon_0)/T]$ is the fugacity, $g_\nu(z) = \sum_{l=1}^{\infty} z^l/l^\nu$ is the Bose-Einstein function, and $\lambda = [1/2\Gamma(d-1)][\sum_{i=1}^d \omega_i/(\prod_{i=1}^d \omega_i)^{1/d}]$ is the coefficient related to the individual oscillator frequency, with gamma function $\Gamma(x) = (x-1)!$. Here, μ and ε_0 denote the chemical potential and ground-state energy, respectively.

By introducing the dimensionless parameters ϕ_i associated with the form of the trapping potential, we set the frequency of the i th ($i = 1, 2, \dots, d$) axis ω_i as $\omega_i = \phi_i \omega^0$, with ω_0 being related to the potential size, and we have $\Omega = \omega^0 (\prod_{i=1}^d \phi_i)^{1/d}$ and $\lambda = [1/2\Gamma(d-1)][\sum_{i=1}^d \phi_i/(\prod_{i=1}^d \phi_i)^{1/d}]$. Note that given dimension d , the coefficient λ is dependent on the set of the parameters $\{\phi_i\}$ only. For example, in the special case when the trapping potential is isotropic, the arithmetic and geometric means of $\{\phi_i\}$ are thus equal to each other, leading to the constant coefficient $\lambda = d/[2\Gamma(d-1)]$. At constant pressure, Bose-Einstein condensation occurs when the system temperature T is lower than the critical temperature $T_c^{\mathcal{P}}$, which reads

$$T_c^{\mathcal{P}} = \left[\frac{\mathcal{P}}{\mathcal{X}}\right]^{1/(d+1)}, \quad (4)$$

where we have used $\mathcal{X} = \zeta(d+1) + \frac{\Gamma(d)}{d} \lambda \frac{\zeta(d)^{1+1/d}}{N^{1/d}} \times [1 - \frac{\Gamma(d-1)\lambda\zeta(d-1)}{d\zeta(d)^{1-1/d}N^{1/d}}]^{-1}$, with $\zeta(d) \equiv g_d(z=1)$ being the Riemannian zeta function [43]. The thermodynamic limit where $N \rightarrow \infty$ leads to $\mathcal{X} = \zeta(d+1)$. The detailed deviation of Eqs. (1)–(4) can be found in Appendix A. Note that for a d -dimensional system with particle number N , \mathcal{X} is kept constant due to fixed λ .

Additionally, in Appendix B, we show that the equation of state [64] for the ideal trapped Bose gas can be given by

$$\mathcal{P}\mathcal{V} = NTF(z), \quad (5)$$

where \mathcal{V} is the so-called “harmonic volume” [62] satisfying $\mathcal{V} = \Omega^{-d}$, and the correction factor is

$$F(z) = \begin{cases} \frac{\mathcal{X}/t^d}{g_d(z) + \frac{d}{d-1} \frac{g_{d-1}(z)}{g_d(z)} [\mathcal{X}/t^d - g_{d+1}(z)]}, & t > 1 \\ \frac{\zeta(d+1) + \mathcal{X}_t}{\zeta(d) + \frac{d\zeta(d-1)}{(d-1)\zeta(d)} \mathcal{X}_t} \left(\frac{\Gamma(d)\lambda\zeta(d)}{\mathcal{X}_t d}\right)^{d-1} \\ \times \left[\frac{\Gamma(d)\lambda\zeta(d)^2}{\mathcal{X}_t N d} + \frac{\lambda\zeta(d-1)}{N}\right], & t \leq 1. \end{cases} \quad (6)$$

Here we have used $t = T/T_c^{\mathcal{P}}$ to denote the reduced temperature [43] and introduced $\mathcal{X}_t \equiv \mathcal{X}/t^{d+1} - \zeta(d+1)$. In contrast to \mathcal{X} and λ , the system volume $\mathcal{V} = 1/[(\omega^0)^d \prod_{i=1}^d \phi_i]$ can be changed by tuning ω_0 when the dimension and form of trapping potential are given, implying that the system volume \mathcal{V} could be changed during an isobaric or adiabatic process with constant λ and \mathcal{X} .

With consideration of Eqs. (2) and (3), the enthalpy \mathcal{H} can be obtained as

$$\mathcal{H} = U + \mathcal{P}\mathcal{V} = (1+d)\mathcal{P}\mathcal{V}. \quad (7)$$

The heat capacity of the system at constant pressure can be determined according to

$$C_{\mathcal{P}} = \left(\frac{\partial \mathcal{H}}{\partial T}\right)_{N, \mathcal{P}}. \quad (8)$$

B. Expressions for efficiency and power

The Brayton engine cycle works between the hot reservoir of temperature T_h and cold reservoir of temperature T_l , as sketched in Fig. 1. During the adiabatic compression (expansion) $1 \rightarrow 2$ ($3 \rightarrow 4$), the system is isolated from the two heat

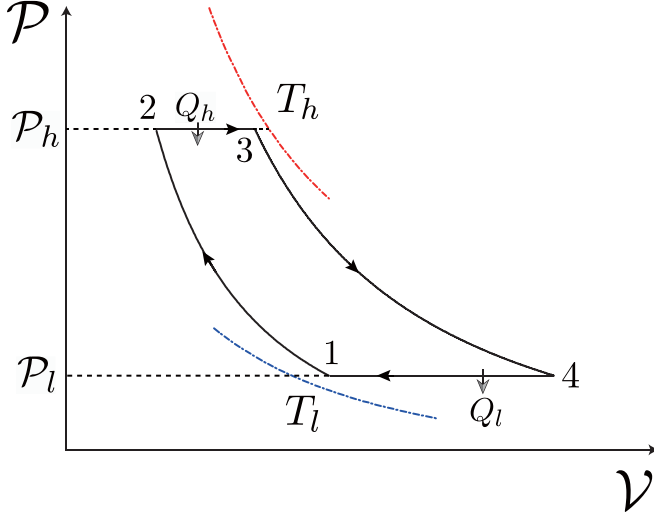


FIG. 1. Pressure vs volume diagram for the endoreversible Brayton cycle. The system is in contact with the hot (cold) reservoir of constant temperature T_h (T_l) during the isobaric expansion ($2 \rightarrow 3$) (isobaric compression $4 \rightarrow 1$). At points 3 and 1, the system temperatures T_3 and T_1 deviate from the reservoir temperatures T_h and T_l due to finite-time operation, but they reach the reservoir temperatures T_h and T_l , respectively, if these two isobaric strokes are reversible. In the isobaric processes $2 \rightarrow 3$ and $4 \rightarrow 1$, the pressures are kept as constants, \mathcal{P}_h and \mathcal{P}_l , respectively.

reservoirs and no heat is exchanged between the system and its surroundings. In the isobaric expansion (compression) $2 \rightarrow 3$ ($4 \rightarrow 1$) proceeding in a time period τ_h (τ_l) with constant pressure \mathcal{P}_h (\mathcal{P}_l), the system is weakly coupled to the hot (cold) reservoir. We assume that this machine cycle consisting of two isobaric and two adiabatic processes is endoreversible, and the total time required for completing the adiabatic strokes is proportional to the total time spent on the two isobaric strokes. That is, the total cycle period can be given by $\tau_{\text{cyc}} = \beta(\tau_h + \tau_l)$. Because of finite-time operation, the system temperatures at the respective ends of isobaric compression and expansion, T_1 and T_3 , deviate from the temperatures of the cold and hot reservoirs, T_l and T_h .

During the isobaric process, the infinitesimal heat exchange between the system and the heat reservoir is given as $\delta Q = C_{\mathcal{P}} dT$, where $C_{\mathcal{P}}$ was defined by Eq. (8). When we introduce the reduced temperature $t = T/T_c^{\mathcal{P}}$, where $T_c^{\mathcal{P}}$ was defined by Eq. (4), we show in Appendix C that the reduced temperature t is kept constant during an adiabatic process. Thus, for the adiabatic compression and expansion, we have $t_1 = t_2$ and $t_3 = t_4$, where $t_{1,4} = T_{1,4}/T_c^{\mathcal{P}_l}$ and $t_{2,3} = T_{2,3}/T_c^{\mathcal{P}_h}$. The heats exchanged during the two isobaric strokes can be determined by using $\delta Q = C_{\mathcal{P}} dT$ to arrive at

$$Q_h = \frac{T_3}{t_3} \int_{t_1}^{t_3} C_{\mathcal{P}} dt, \quad Q_l = \frac{T_1}{t_1} \int_{t_1}^{t_3} C_{\mathcal{P}} dt. \quad (9)$$

In deriving Eq. (9), we have used the conditions of $t_1 = t_2$ and $t_3 = t_4$ holding in the adiabatic compression and expansion. With consideration of Eqs. (7)–(9), the heat input to the system along the hot isobaric process and the heat output from

the system along the cold isobaric process read

$$Q_h = (d+1)\mathcal{P}_h(\mathcal{V}_3 - \mathcal{V}_2), \quad Q_l = (d+1)\mathcal{P}_l(\mathcal{V}_4 - \mathcal{V}_1). \quad (10)$$

As there is no heat exchange during the two adiabatic strokes, the total work output per cycle is given as $W = Q_h - Q_l$. By introducing the adiabatic exponent $\gamma = (d+1)/d$, we can prove that the relation $\mathcal{V}\mathcal{P}^{\frac{1}{\gamma}} = \text{const}$ during the adiabatic compression or expansion (see, also, Appendix C). It follows that using Eq. (5) and the condition $\mathcal{V}\mathcal{P}^{\frac{1}{\gamma}} = \text{const}$ during an adiabatic stroke, the work output per cycle is given by

$$W = N(1+d) \left(\frac{1}{r} - 1 \right) [rT_3 F(z_3) - T_1 F(z_1)], \quad (11)$$

where we have introduced the compression ratio $r \equiv (\mathcal{P}_l/\mathcal{P}_h)^{1-1/\gamma}$ and F_z ($z = z_1, z_3$) was given by Eq. (6). The thermodynamic efficiency [65,66], $\eta = W/Q_h$, can be derived by using Eqs. (11) and (10), yielding

$$\eta = 1 - r. \quad (12)$$

This efficiency for the quantum Brayton engine takes the same expression as that for the classical counterpart [19,67]. With consideration of Eq. (4), the ratio r defined in Eq. (11) can be reexpressed as $r = T_c^{\mathcal{P}_l}/T_c^{\mathcal{P}_h}$. The ratio r can be rewritten as $r = t_h T_l / (t_l T_h)$, if the reduced temperatures $t_{l,h} = T_{l,h}/T_c^{\mathcal{P}_{l,h}}$ are introduced. Thus, the efficiency (12) also takes the form of $\eta = 1 - t_h T_l / (t_l T_h)$.

We assume that the system temperature at time τ during the isobaric process satisfies Fourier's law [68,69],

$$\dot{T}(\tau) = -\kappa_v [T(\tau) - T_v], \quad (13)$$

where the dot on top denotes the instantaneous rate of change of temperature $T(\tau)$ with respect to time τ , and κ_v denotes the thermal conductivity between the system and the heat reservoir of temperature T_v , with $v = l, h$. Using Eq. (13), we have

$$T_3 - T_h = (T_2 - T_h) \exp(-\kappa_h \tau_h), \quad (14)$$

$$T_1 - T_l = (T_4 - T_l) \exp(-\kappa_l \tau_l). \quad (15)$$

These two equations, together with the relation $T\mathcal{P}^{\frac{1}{\gamma}-1} = \text{const}$ during the two adiabatic strokes, give rise to

$$\tau_l = \frac{1}{\kappa_l} \ln \left(\frac{rT_3 - T_l}{T_1 - T_l} \right), \quad \tau_h = \frac{1}{\kappa_h} \ln \left(\frac{T_1/r - T_h}{T_3 - T_h} \right) \quad (16)$$

or

$$\tau_l = \frac{1}{\kappa_l} \ln \left(\frac{t_3 - t_l}{t_1 - t_l} \right), \quad \tau_h = \frac{1}{\kappa_h} \ln \left(\frac{t_1 T_l - r t_l T_h}{t_3 T_l - r t_l T_h} \right). \quad (17)$$

In terms of t_1 and t_3 , the work output given as Eq. (11) can be reexpressed as $W = N(1+d) \frac{T_l}{t_1} \left(\frac{1}{r} - 1 \right) [t_3 F(z_3) - t_1 F(z_1)]$. Using Eq. (17), it follows that the power output, $P = W/\tau_{\text{cyc}}$, can be obtained as

$$P = \frac{N(1+d)(1-r)\kappa_h \kappa_l T_l [t_3 F(z_3) - t_1 F(z_1)]}{\beta r t_l \left[\ln \left(\frac{t_3 - t_l}{t_1 - t_l} \right) \kappa_h + \ln \left(\frac{t_1 T_l - r t_l T_h}{t_3 T_l - r t_l T_h} \right) \kappa_l \right]}. \quad (18)$$

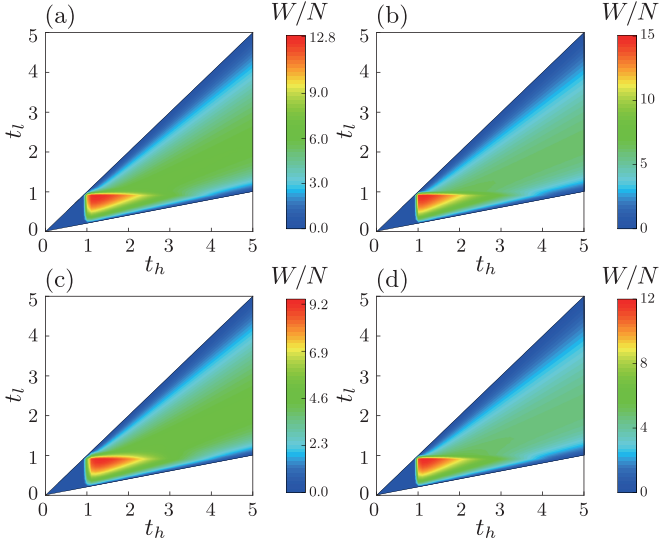


FIG. 2. Contour plots of work per particle W/N as a function of reduced temperatures t_h and t_l for a d -dimensional ideal Bose gas with a finite particle number N in the quasistatic limit. In (a) and (b), $d = 3$, but $N = 200$ in (a) and $N = 2000$ in (b). In (c) and (d), $d = 2$, but $N = 200$ in (c) and $N = 2000$ in (d). The other parameters are $T_l = 1$ and $T_h = 5$.

C. Work and power output in the three different working regimes

No Bose-Einstein condensation can occur during an adiabatic process of constant fugacity (see Appendix C for details). The heat engine in each cycle may operate in the three regimes: a full condensation regime, a complete out-of-condensation regime, and a near-critical point regime with the cycle proceeding across the Bose-Einstein condensation that occurs along an isobaric process.

In the quasistatic limit where time periods τ_l and τ_h are quite long, the system temperatures at the ends of two isobaric strokes are close to the respective temperatures of the two heat reservoirs, $T_3 \rightarrow T_h$ and $T_1 \rightarrow T_l$. In a quasistatic cycle, using Eq. (9), the total work output can be expressed as

$$W = \left(\frac{T_h}{t_h} - \frac{T_l}{t_l} \right) \int_{t_l}^{t_h} C_{\mathcal{P}} dt, \quad (19)$$

with $t_h \equiv T_h/T_c^{\mathcal{P}_h}$. Without loss of generality, in the following we will present a numerical analysis of the machine performance with focus on the case when the trapping potential is isotropic. The condition of $t_h \geq t_l$ must be satisfied in order for the machine to be operated as a heat engine producing positive work, as shown in Figs. 2(a)–2(d), where $d = 2, 3$ [70]. The working medium of the thermal machine may be in three different regimes: a complete condensation regime where $t_{h,l} < 1$, a near-critical point regime where $t_l < 1$ and $t_h \gtrsim 1$, and a complete noncondensation case with $t_{h,l} > 1$. The machine working either in the condensed phase when $t_{h,l} < 1$ or in the noncondensed phase with $t_{h,l} > 1$ produces smaller work output than that in the working regime close to the critical point. That is, the largest values of work per particle are observed in the working regime near the transition point, demonstrating phase-transition supremacy of the

thermal machine. We also see from Figs. 2(a) and 2(b) [Figs. 2(c) and 2(d)] that given dimensional d , the work per particle increases with increasing particle number N . Comparison between Figs. 2(a) and 2(c) [Figs. 2(b) and 2(d)] shows that given particle number N , higher-dimensional working systems show better performance, producing larger work per particle.

Given the reduced temperature t_l , the work output per particle as a function of t_h for $d = 3$ and $N = 200, 2000, 20000$ (for $N = 200$ and $d = 2, 3$) is shown in the upper (lower) panel of Figs. 3(a)–3(c). While the full condensation (noncondensation) regime is plotted in Fig. 3(a) [3(b)], the near-critical point regime is shown in Fig. 3(c). In contrast to the Otto engine cycle [24], the work per particle is particularly small in the complete condensation regime due to very small heat exchanged between the system and its surroundings, as can be seen in Fig. 3(a). This makes the Brayton engine cycle, operating in the condensation phase, a very marginal machine that will not be discussed in the following. By contrast, the exhibition of a phase transition between the condensation and noncondensation phases during a machine cycle significantly enhances the work output, as shown in Fig. 3(c). For the heat engine working either in the Bose-Einstein condensation phase or in the noncondensation regime, the work output per particle, W/N , decreases as particle number N increases [cf. Figs. 3(a) and 3(b)]. However, the work output per particle, W/N , for the machine operating across the Bose-Einstein condensation is increasing with increasing particle number N [see Fig. 3(c)]. Therefore, the quantum engine working across the phase transition in the many-particle Bose system is superior to an ensemble of independent single-particle machines. As is well known, the wave functions of neighboring particles in a Bose gas begin to overlap if the temperature is lowered. When the temperature is sufficiently low, the particles are coupled to each other and coalesce into a single quantum entity with a common wave function, leading to the formation of Bose-Einstein condensation. Therefore, the heat engine with Bose-Einstein condensation under consideration, as an array of individual heat engines under the condition of an appropriate interparticle coupling, produces superior work output to that of an ensemble of independent single-particle engines.

This distinction among these figures can be explained by the behavior of the specific heat at constant pressure associated with heat injection during an isobaric stroke. In Appendix D, we analyze the specific heat of the Bose gas with a finite number of particles confined in a d -dimensional harmonic trap; we show that the specific heat shows a cusp (which becomes divergent in the thermodynamic limit [71,72]) at the critical point is much larger than that both in the condensation phase and in the noncondensation regime. In physical terms, at the critical point, the majority of the heat injection is not responsible for heating up, but rather for creating the phase transition, thereby implying that a finite heat would be exchanged only with an infinitesimal change in temperature. For increasing temperature ΔT , compared to the system with higher specific heat, the system with lower heat capacity absorbs less energy per unit particle. Due to the singularity of the specific heat at the critical point, the work output in the near-critical point regime is larger compared to that in the condensation and noncondensation regimes.

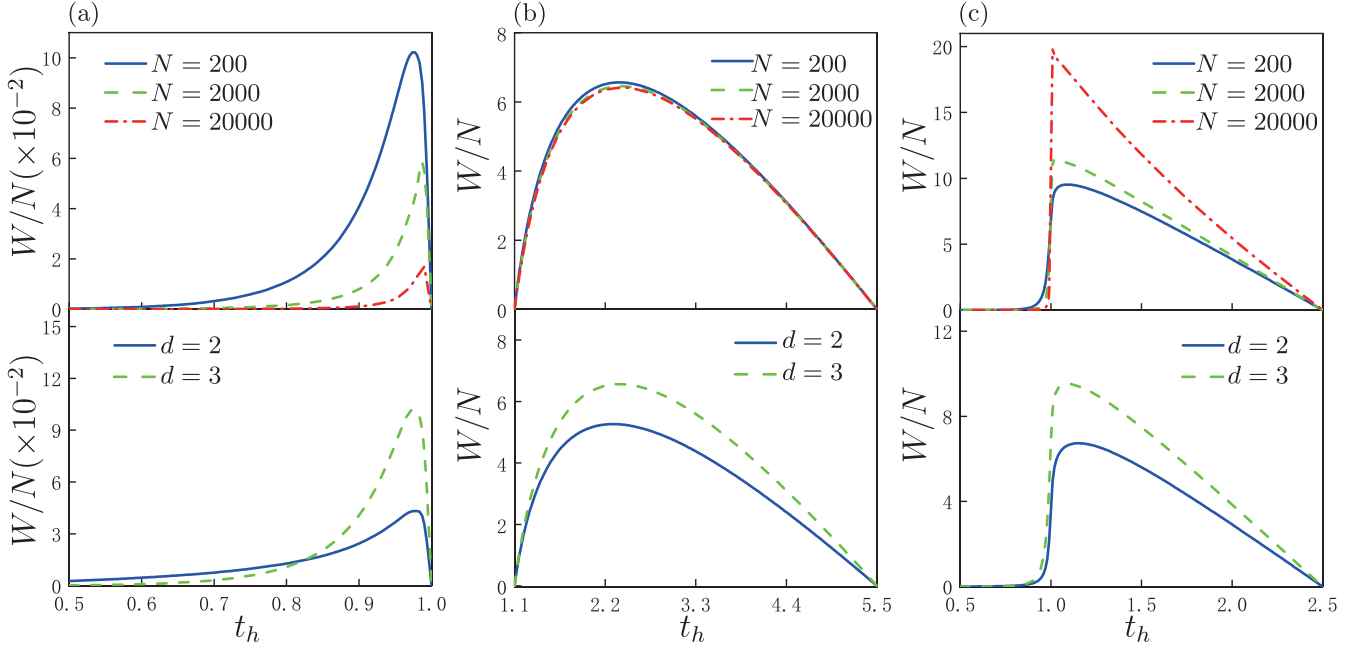


FIG. 3. The work per particle as function of t_h for the Brayton heat engine operating in three different regimes: (a) complete condensation regime with $t_l = 0.2$, (b) out-of-condensation regime with $t_l = 1.1$, and (c) near-critical point regime with $t_l = 0.5$. While the upper panels of these figures are plotted for $d = 3$ and $N = 200, 2000, 20000$, the lower panels are shown for $N = 200$ and $d = 2, 3$. The other parameters are $T_l = 1$ and $T_h = 5$.

Therefore, when passing the transition point, the machine produces the maximal work output [see Fig. 3(c)].

Unlike in the regime away from the critical point, the work per particle can be enhanced by increasing the particle number when the machine drives across the critical point. This follows from the fact that while in both full condensate and noncondensate regimes the specific heat per particle at constant pressure is decreasing with increasing particle, in the regime near the transition point, the specific heat per particle is increasing with increasing particle number. For a given particle number, as the dimensionality increases, the specific heat at the critical point becomes sharper and its peak becomes greater. The work output per particle increases with increasing dimensionality, as it should [see the lower panel of Figs. 3(a)–3(c)].

From Eq. (14) [(15)], we find that the system temperature T_3 (T_l) deviates from the reservoir temperature T_h (T_l) due to finite-time duration τ_h (τ_l). Unlike in the quasistatic limit where the values of $t_{h,l}$ determine the working regimes, the working regimes for the heat engine in finite time are dependent on the values of $t_{3,1}$. For finite-time operation, the relations of $t_{1,3} < 1$, $t_1 < 1 \lesssim t_3$, and $t_{1,3} > 1$ correspond to the full condensation regime, near-critical point regime, and noncondensation regime, respectively. It is an interesting question whether or not the power output can be enhanced by the phase transition. In order to answer this, we compare the power output in the near-critical point regime with those in the regimes away from the critical point by plotting the power per particle as a function of reduced temperature t_3 . This comparison is shown in Fig. 4. Apparently, the behavior of power output for finite-time operation is similar to that work in the quasistatic case. The power output, like the work output, is larger in the three-dimensional case than in

the two-dimensional case. The power output in the complete condensation phase is extremely low due to particularly small work, as shown in Fig. 4(a), implying again that this working regime is of no meaningful application. Figures 4(b) and 4(c) show that the machine working across the phase transition produces much higher power than its counterpart with no phase transition, demonstrating that Bose-Einstein condensation can boost the power output of the machine.

D. Maximum power and maximum efficient power with respect to corresponding efficiencies

To consider the effects of phase transition on the performance of the heat engine in finite time, we consider both power and efficiency by comparing the three working regimes: (i) the near-critical point regime when the machine operates with the cycle passing through the Bose-Einstein condensation with $t_1 < 1 < t_3$, (ii) the out-of-condensation, finite-temperature regime where the temperature of the system is higher than the critical temperature, but not by much, namely, $t_{1,3} > 1$, and (iii) the regime of high temperatures where $t_{1,3} \gg 1$. The power output (18) as a function of the efficiency (12) is shown in Fig. 5(a). For a given working regime, there is a maximal power output P_{\max} that determines the optimal efficiency η^* . We see that the power output in the noncondensation regime (red dashed line) lies close to the corresponding one in the high-temperature limit (black short-dashed line), and the difference of the efficiencies at maximum power between these two cases is small. By contrast, both the power output and the efficiency at maximum power are much higher in the near-critical regime than both in the out-of-condensation regime and in the high-temperature limit. This can be understood by the fact that the exhibition

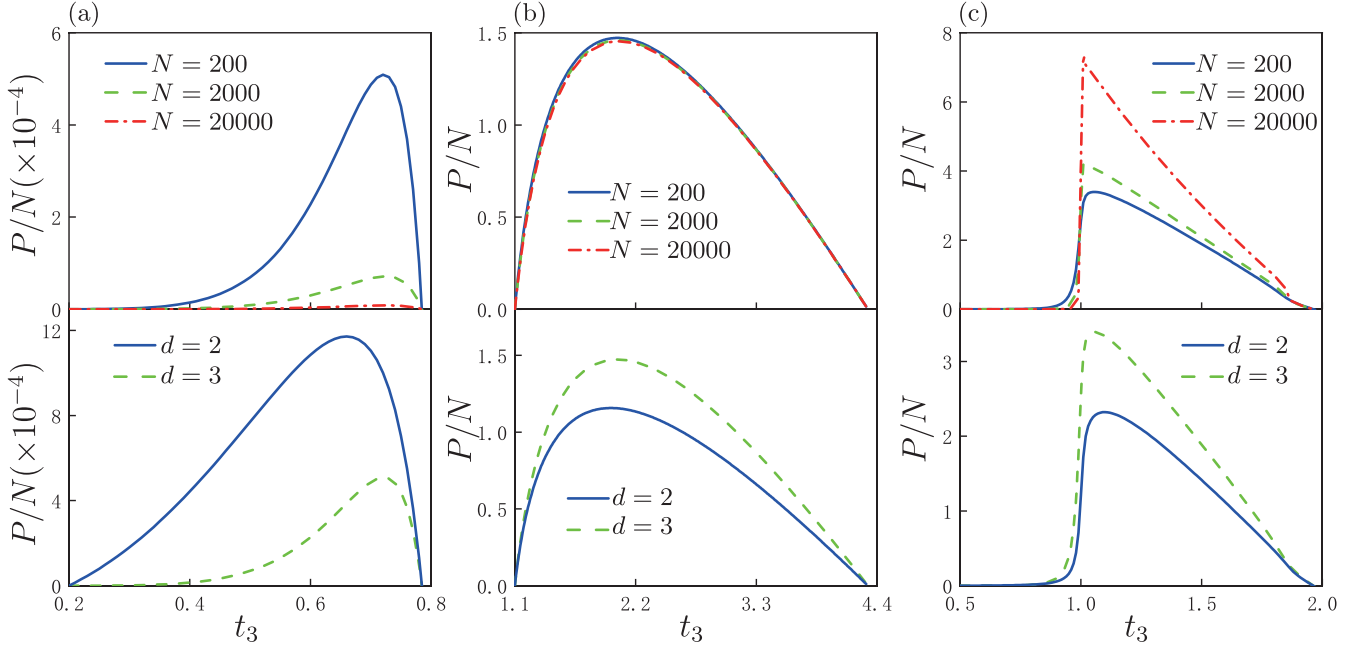


FIG. 4. The power per particle as function of t_3 for the Brayton heat engine operating in three different regimes: (a) complete condensation regime with $t_l = 0.2$, (b) out-of-condensation regime with $t_l = 1.1$, and (c) near-critical point regime with $t_l = 0.5$. While the upper panels of these figures are plotted for $d = 3$ and $N = 200, 2000, 20000$, the lower panels are shown for $N = 200$ and $d = 2, 3$. The other parameters are $T_l = 1, T_h = 5, \kappa_l = \kappa_h = 1, \beta = 1$, and $\tau_h = \tau_l = 1$. Note that given these parameters, t_l and t_h can be numerically determined by substituting the relation $r = t_h T_l / (t_l T_h)$ into Eq. (17).

of the phase transition significantly enhances the power output. The efficiency $\eta = 1 - r = 1 - t_h T_l / (t_l T_h)$ approaches the Carnot efficiency in the extremal case $t_h \rightarrow t_l$. At this limit, the machine under consideration runs at the efficiency equal to the efficiency of the ideal Carnot engine, but it produces vanishing work and thus null power [73].

To consider the efficiency for the heat engine under maximal power, we numerically determine the maximal value of power output [cf. Eq. (18)] and the corresponding efficiency (η^*) through optimal control of external parameters that include the parameters r, t_2, t_3 (see Appendix E for details).

In Fig. 5(b), numerical results are reported for the values of efficiency at maximum power as a function of Carnot efficiency η_C in the near-critical point regime (η_{crit}^*), and out-of-condensation regime (η_{hcrit}^*) in which the temperature is not much higher than the critical temperature, compared with the CA efficiency η_{CA} . When the engine operates in the noncondensation regime but with temperature slightly higher than the critical temperature, the efficiency at maximum power is observed to be higher than the CA efficiency. Crucially, the efficiency at maximum power is much higher than the CA efficiency when the machine cycle passes through the

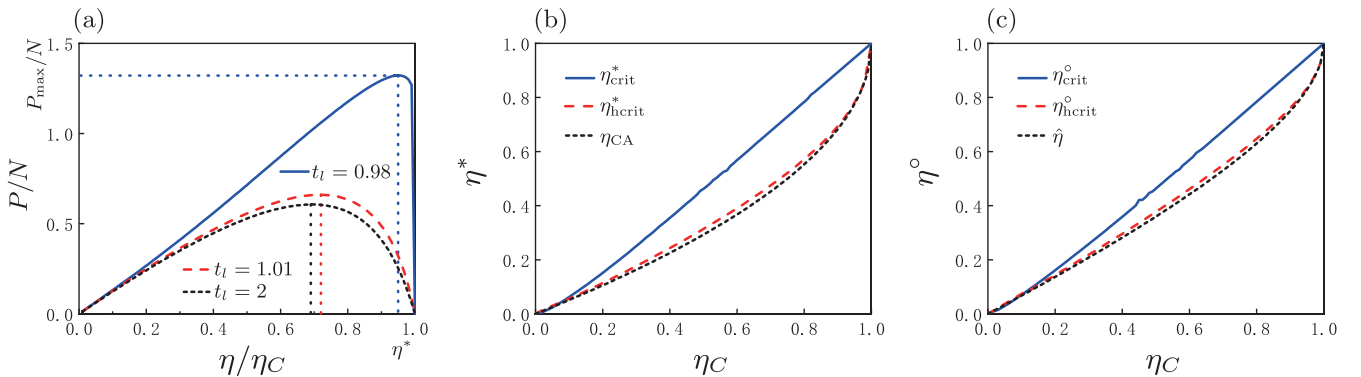


FIG. 5. (a) Power as a function of reduced efficiency η/η_C , with the Carnot efficiency η_C . (b),(c) The efficiencies corresponding to (b) the maximum power and (c) the maximum efficiency power vs the Carnot efficiency η_C , for the machine operating in the near-critical point regime (blue solid line) where $t_l = 0.98$, in the noncondensation regime (red dashed line) where $t_l = 1.01$, and (black short dashed line) reproduced in the high-temperature limit where $t_l = 2$. In (a), the vertical dotted line pattern (black, red, and blue) indicates the maximum power corresponding to the ratio of efficiency to Carnot efficiency ($\eta/\eta_C = 0.691, \eta/\eta_C = 0.724, \eta/\eta_C = 0.951$). In (a), the parameters are $T_l = 1, T_h = 5$, and $\tau_h = \tau_l = 5$. The other parameters are $\kappa_l = \kappa_h = 1$ and $\beta = 1$.

Bose-Einstein condensation. The efficiency at maximum power in such a case, not limited by the CA bound, $\eta_C/2 + \eta_C^2/8$ [50], can approach the Carnot limit due to the phase transition that accounts for improved finite-time performance (see Appendix F for the explanation). Noteworthy, we find that the efficiency at maximum power in the high-temperature regime is identical to the CA efficiency η_{CA} that is indicated by the black short-dashed line in Fig. 5(b). This is the expected result since the quantum Brayton cycle turns out to be the classical endoreversible model in the high-temperature limit where the state function becomes the classical form $\mathcal{P}\mathcal{V} = NT$.

The efficient power as the product of power and efficiency is given by $\Theta = P\eta$, where P and η were given by Eqs. (18) and (12), respectively. The efficient power Θ can be used as another objective optimization criterion, in which the trade-off between efficiency and power is involved. The efficiency at maximum efficient power can be determined following the same approach that we used to determine the efficiency at maximum power, and thus we set $\{\partial\Theta/\partial t_1 = 0, \partial\Theta/\partial t_3 = 0, \partial\Theta/\partial r = 0\}$ to obtain the optimal values of t_1 , t_3 , and r , as well as the optimal efficiency η° . Our numerical result shows that the efficiency for the engine under maximal efficient power behaves similarly to the efficiency at maximum power [see Fig. 5(c)]. We observe that, the efficiency at maximum efficient power in the near-critical point regime (η_{crit}°) is much larger than the corresponding ones in both the out-of-condensation, finite-temperature regime ($\eta_{\text{hcrit}}^\circ$) and the high-temperature limit $\hat{\eta}$, whereas the optimal efficiency $\eta_{\text{hcrit}}^\circ$ is only slightly higher than the optimized efficiency $\hat{\eta}$. Like the power output (see Appendix E), the efficient power Θ be reexpressed in terms of τ_l and τ_h : $\Theta = 2NT_h(1+d)(1-r)(\frac{1}{r} - 1)(r + \eta_C - 1) \times \frac{\sinh(\kappa_l \tau_l/2) \sinh(\kappa_h \tau_h/2)}{\beta(\tau_h + \tau_l) \sinh[(\kappa_h \tau_h + \kappa_l \tau_l)/2]}$. The system of equations $\{\partial\Theta/\partial \tau_h = 0, \partial\Theta/\partial \tau_l = 0\}$ gives the same optimal time allocations τ_h and τ_l as those in maximizing power output. We then use $\partial\Theta/\partial r = 0$ to obtain the efficiency at maximum efficient power as $\hat{\eta} = [3 + \eta_C - \sqrt{(\eta_C - 9)(\eta_C - 1)}]/4$, which was previously obtained from Carnot-like engines based on endoreversible [59,60] or low-dissipation [74] assumption.

As emphasized, the results for efficiency at maximum power and efficiency at maximum efficient power are valid for all non-one-dimensional systems and all particle numbers, which are therefore universal for any non-one-dimensional, finite-size Bose systems.

As a final remark, a quantum Brayton engine may be experimentally implemented by alternatively coupling an extremely dilute gas of cold atoms confined in a harmonic trap to two bosonic heat baths of different temperatures. We focus on a finite number of cold atoms confined in a harmonic trap because of its relevance to the realized experiments [38,75,76]. Thermodynamic transformations are achieved by accurately controlling and also tuning off the weak interaction between the system and heat bath. During an isobaric process, the system of trapped cold atoms is weakly coupled to a boson bath. The bath Hamiltonian reads $\hat{H}_B = \sum_k \omega_k \hat{b}_k^\dagger b_k$, where \hat{b}_k and \hat{b}_k^\dagger are the annihilation and creation operators for a mode k [77]. The bath may include a photon bath (the electromagnetic field) or a phonon bath (a macroscopic piece of solid), or a thermal cloud of ultracold atoms (a species of cold atoms

different from the working system [78]). An adiabatic stroke is performed through adiabatically changing the trap frequency Ω via the power of the laser forming the trapping potential, during which work is thus performed. Approximate adiabatic dynamics in the experiment requires a very slow change of the control Hamiltonian, leading to no net change in the population of the instantaneous energy levels. We further change the external field through varying trap frequency together with the temperature to realize an isobaric process along which both heat dissipation and work are produced. The temperature that can be measured is changed while satisfying the condition that the pressure, given by Eq. (3) (in which the fugacity z is determined by frequency and temperature for constant particle number), is kept constant.

III. CONCLUSION

In summary, we have theoretically analyzed a Brayton engine which uses an ideal Bose gas with a finite number of particles confined in a d -dimensional harmonic trap as its working substance. Our analysis shows that the engine working across the Bose-Einstein-condensation transition point can outperform its nontransition counterpart by dramatically enhancing power output and efficiency at maximum power or maximum efficient power. While the efficiency at maximum power is independent of particle number N , the Bose-Einstein condensation as an appropriate form of coupling may boost the power output, which leads to the power output surpassing that of an ensemble of independent single-particle quantum heat engines. Our findings demonstrated the potential of many-particle quantum heat engines utilizing phase transition with singularity of physical quantities to realize ideal thermal machines with an overall good performance.

ACKNOWLEDGMENTS

This work is supported by the National Natural Science Foundation of China under Grants No. 11875034 and No. 12175040. J.W. acknowledges the financial support from the Major Program of Jiangxi Provincial Natural Science Foundation under Grant No. 20224ACB201007, and the Opening Project of Shanghai Key Laboratory of Special Artificial Microstructure Materials and Technology. Y.M. acknowledges financial support from the State Key Programs of China under Grant No. 2017YFA0304204.

APPENDIX A: BOSE-EINSTEIN CONDENSATION THERMODYNAMICS

Let us consider an ideal Bose gas with a finite number of particles confined in a d -dimensional harmonic trap, of which the frequencies along the x_1, x_2, \dots and x_d axis are $\omega_1, \omega_2, \dots$ and ω_d , respectively. By using a grand-canonical-ensemble treatment, the mean population of the Bose system with temperature T and chemical potential μ can be expressed as ($k_B \equiv 1$)

$$n_i = \frac{1}{\exp[(\varepsilon_i - \mu)/T] - 1}, \quad (\text{A1})$$

with $\mathbf{i} = \{i_1, i_2, \dots, i_d\}$ being nonzero integers. Here the single-particle energies ε_i take the following form ($\hbar \equiv 1$): $\varepsilon_i = \sum_j \mathbf{i} \omega_j + \varepsilon_0$, with ground-state energy $\varepsilon_0 = \sum_j \omega_j/2$ with $j = 1, 2, \dots, d$. The particle conservation $N = \sum_i n_i$ should be satisfied.

The density of states with the geometric mean of the oscillator frequencies $\Omega = (\prod_{d=1}^d \omega_i)^{1/d}$ is given by [41]

$$\rho(E) = \frac{E^{d-1}}{\Gamma(d)\Omega^d} + \lambda \frac{E^{d-2}}{\Omega^{d-1}}, \quad (\text{A2})$$

where $\lambda = [1/2\Gamma(d-1)]/[\sum_{i=1}^d \omega_i/(\prod_{i=1}^d \omega_i)^{1/d}]$ is the coefficient related to the individual oscillator frequency, with $\Gamma(x) = (x-1)!$ the gamma function. When the particle number N is sufficiently large, the second term in Eq. (A2) can be neglected. This term, however, plays an important role, as it accounts for the correction due to finite particle number N [41,43,62].

Using the identity $N - N_0 = \int_0^\infty \rho(E)n(E)dE$, we obtain the total number of particles [63] as

$$N = N_0 + \left(\frac{T}{\Omega}\right)^d g_d(z) + \lambda\Gamma(d-1)\left(\frac{T}{\Omega}\right)^{d-1} g_{d-1}(z), \quad (\text{A3})$$

where $N_0 = z/(1-z)$ is the ground-state occupation number, with the fugacity $z = \exp[(\mu - \varepsilon_0)/T]$, and $g_\nu(z) = \sum_{l=1}^\infty z^l/l^\nu$ indicates the Bose-Einstein function. As $0 \leq z < 1$, the function $g_\nu(z)$ is bounded by $g_\nu(1) = \zeta(\nu)$, where $\zeta(\nu)$ is the Riemannian zeta function.

The logarithm of the grand partition function [64] for an ideal Bose system confined in harmonic trap is given by

$$\ln \Xi = - \sum_{\varepsilon_i} \ln \{1 - \exp[(\mu - \varepsilon_i)/T]\}. \quad (\text{A4})$$

By using $\ln \Xi = - \int_0^\infty \rho(E) \ln \{1 - \exp[(\mu - \varepsilon_0 - E)/T]\} dE$, the logarithm of the grand partition function can be obtained as

$$\ln \Xi = \left(\frac{T}{\Omega}\right)^d g_{d+1}(z) + \lambda\Gamma(d-1) \times \left(\frac{T}{\Omega}\right)^{d-1} g_d(z) - \ln(1-z), \quad (\text{A5})$$

which determines the grand thermodynamic potential $\mathcal{G} = -T \ln \Xi$. Employing the identity $U = T^2(\partial \ln \Xi / \partial T)_{z, \Omega}$, it follows that the internal energy U reads

$$U = Td \left(\frac{T}{\Omega}\right)^d g_{d+1}(z) + \lambda\Gamma(d)T \left(\frac{T}{\Omega}\right)^{d-1} g_d(z). \quad (\text{A6})$$

Introducing the ‘‘harmonic volume’’ $\mathcal{V} = \Omega^{-d}$ [62], we can determine the pressure \mathcal{P} by using the identity $\mathcal{P} = -(\partial \mathcal{G} / \partial \mathcal{V})_{z, T}$ to arrive at

$$\mathcal{P} = T^{d+1} g_{d+1}(z) + \lambda \frac{\Gamma(d)}{d} \Omega T^d g_d(z). \quad (\text{A7})$$

In the condensation phase, the fugacity of the system satisfies $z \approx 1$, and the ground-state particle number (A3) can be

reexpressed as

$$N_0 = N - \left(\frac{T}{\Omega}\right)^d \zeta(d) - \lambda\Gamma(d-1) \left(\frac{T}{\Omega}\right)^{d-1} \zeta(d-1). \quad (\text{A8})$$

At the critical point of the phase transition, $N_0 \approx 0$. It follows, using Eq. (A8), that the ratio of the critical temperature $T_c^{\mathcal{P}}$ to the critical frequency $\Omega_c^{\mathcal{P}}$ at constant pressure can be obtained,

$$\frac{T_c^{\mathcal{P}}}{\Omega_c^{\mathcal{P}}} \approx \left(\frac{N}{\zeta(d)}\right)^{1/d} \left[1 - \frac{\Gamma(d-1)\lambda\zeta(d-1)}{d\zeta(d)^{1-1/d}} \frac{1}{N^{1/d}}\right]. \quad (\text{A9})$$

At the phase transition point, the pressure (A7) becomes

$$\mathcal{P} = (T_c^{\mathcal{P}})^{d+1} \zeta(d+1) + \lambda \frac{\Gamma(d)}{d} \Omega_c^{\mathcal{P}} (T_c^{\mathcal{P}})^d \zeta(d). \quad (\text{A10})$$

With consideration of Eqs. (A9) and (A10), the transition temperature for the finite Bose system at constant pressure is obtained as Eq. (4).

APPENDIX B: THE EQUATION OF STATE

Here we analyze the equation of state for the Bose system [21,64] with particle number N . In the case when the temperature T is not larger than the critical temperature $T_c^{\mathcal{P}}$, and the fugacity $z \approx 1$, the pressure (A7) can be rewritten as

$$\mathcal{P} = T^{d+1} \zeta(d+1) + \lambda \frac{\Gamma(d)}{d} \Omega T^d \zeta(d), \quad (\text{B1})$$

where the second term would be vanishing in the thermodynamic limit. For a large-size Bose system, the isobaric process means the isothermal process. However, this is not the case for the finite-size system where Ω is varied to realize an isobaric stroke. Equation (B1), combining with Eq. (A8), gives rise to

$$\mathcal{P}\mathcal{V} \Big|_{T \leq T_c^{\mathcal{P}}} = NT \frac{\zeta(d+1) + [\Gamma(d)\lambda\Omega/Td]\zeta(d)}{\zeta(d) + [\lambda\Gamma(d-1)\Omega/T]\zeta(d-1)} \times \left[\left(\frac{T}{\Omega}\right)^d \frac{\zeta(d)}{N} + \left(\frac{T}{\Omega}\right)^{d-1} \frac{\lambda\zeta(d-1)}{N} \right]. \quad (\text{B2})$$

Using Eqs. (4) and (B1), we have

$$\frac{\Omega}{T} \Big|_{T < T_c^{\mathcal{P}}} = \frac{d}{\Gamma(d)\lambda\zeta(d)} \left[\frac{\mathcal{X}}{T^{d+1}} - \zeta(d+1) \right]. \quad (\text{B3})$$

Substituting Eq. (B3) into Eq. (B2) leads to

$$\mathcal{P}\mathcal{V} \Big|_{T \leq T_c^{\mathcal{P}}} = NT \frac{\zeta(d+1) + \mathcal{X}_t}{\zeta(d) + \frac{d\zeta(d-1)}{(d-1)\zeta(d)} \mathcal{X}_t} \left(\frac{\Gamma(d)\lambda\zeta(d)}{\mathcal{X}_t d} \right)^{d-1} \times \left[\frac{\Gamma(d)\lambda\zeta(d)^2}{\mathcal{X}_t N d} + \frac{\lambda\zeta(d-1)}{N} \right], \quad (\text{B4})$$

where we have used $\mathcal{X}_t \equiv \mathcal{X}/T^{d+1} - \zeta(d+1)$, with \mathcal{X} as given in Eq. (4).

On the other hand, when the system temperature $T > T_c^{\mathcal{P}}$, the number of particles in the ground state almost disappears, $N_0 \approx 0$. Equations (A3) and (A7) set the equation of state,

$$\mathcal{P}\mathcal{V} = NT \frac{g_{d+1}(z) + [\Gamma(d)\lambda\Omega/Td]g_d(z)}{g_d(z) + [\lambda\Gamma(d-1)\Omega/T]g_{d-1}(z)}. \quad (\text{B5})$$

The relation

$$\frac{\Omega}{T} \Big|_{T > T_c^P} = \frac{d}{\Gamma(d)\lambda g_d(z)} \left[\frac{\mathcal{X}}{t^{d+1}} - g_{d+1}(z) \right] \quad (\text{B6})$$

can be derived from Eqs. (A7) and (4). Substitution of Eq. (B6) into Eq. (B5) yields

$$\mathcal{P}\mathcal{V} \Big|_{T > T_c^P} = NT \frac{\mathcal{X}/t^d}{g_d(z) + \frac{d}{d-1} \frac{g_{d-1}(z)}{g_d(z)} [\mathcal{X}/t^d - g_{d+1}(z)]}. \quad (\text{B7})$$

We therefore conclude that the equation of state for the trapped d -dimensional Bose systems is expressed as Eq. (6).

When $T > T_c^P$, the correction factor simplifies $F(z) \Big|_{T > T_c^P} \xrightarrow{N \rightarrow \infty} \frac{g_{d+1}(z)}{g_d(z)}$ in the thermodynamic limit. At higher temperatures, the correction factor can be approximated by $F(z) \approx 1$ and thus the equation of state turns out to be $\mathcal{P}\mathcal{V} = NT$, as it should [64].

APPENDIX C: ISENTROPIC CONDITION DURING AN ADIABATIC PROCESS

We show that the ratio Ω/T is kept constant during the adiabatic process. Using the grand thermodynamic potential $\mathcal{G} = -T \ln \Xi$, the thermodynamic entropy $S = -(\partial \mathcal{G} / \partial T)_{u, \Omega}$ can be obtained as

$$S = \left(\frac{T}{\Omega} \right)^d [(1+d)g_{d+1}(z) - g_d \ln z(z)] + \lambda \Gamma(d-1) \left(\frac{T}{\Omega} \right)^{d-1} [g_d(z)d - g_{d-1}(z) \ln z]. \quad (\text{C1})$$

During the isentropic, adiabatic process, we obtain

$$dS = \left(\frac{\partial S}{\partial T} \right)_{\Omega} dT + \left(\frac{\partial S}{\partial T} \right)_{T} d\Omega = 0, \quad (\text{C2})$$

leading to

$$\frac{d\Omega}{dT} = - \frac{\left(\frac{\partial S}{\partial T} \right)_{\Omega}}{\left(\frac{\partial S}{\partial \Omega} \right)_{T}}. \quad (\text{C3})$$

Using Eq. (C1) and the relation $dg_v(z)/dz = g_{v-1}(z)/z$, it follows that

$$- \frac{\left(\frac{\partial S}{\partial T} \right)_{\Omega}}{\left(\frac{\partial S}{\partial \Omega} \right)_{T}} = \frac{\Omega}{T} \left(\frac{\Phi + T \frac{\partial \zeta}{\partial T} \Psi}{\Phi - \Omega \frac{\partial \zeta}{\partial \Omega} \Psi} \right), \quad (\text{C4})$$

where we have used $\Phi \equiv d[(1+d)g_{d+1}(z) - g_d \ln z(z)] + \lambda \Omega \Gamma(d)[g_d(z)d - g_{d-1}(z) \ln z]/T$ and $\Psi \equiv [g_d(z)d - g_{d-1}(z) \ln z]/z + \lambda \Omega [\Gamma(d)g_{d-1}(z) - \Gamma(d-1)g_{d-2}(z) \ln z]/(Tz)$.

Due to conservation of the particle number given by (A3), we have $(\partial N / \partial T)_{\Omega} = 0$ and $(\partial N / \partial \Omega)_{T} = 0$ during the adiabatic process, leading to

$$\frac{\partial z}{\partial T} = - \frac{zd}{T} \frac{g_d(z) + [\Gamma(d)\lambda\Omega/Td]g_{d-1}(z)}{\Upsilon + g_{d-1}(z) + [\Gamma(d-1)\lambda\Omega/T]g_{d-2}(z)} \quad (\text{C5})$$

and

$$\frac{\partial z}{\partial \Omega} = \frac{zd}{\Omega} \frac{g_d(z) + [\Gamma(d)\lambda\Omega/Td]g_{d-1}(z)}{\Upsilon + g_{d-1}(z) + [\Gamma(d-1)\lambda\Omega/T]g_{d-2}(z)}, \quad (\text{C6})$$

where we have used $\Upsilon = \frac{z}{(z-1)^2} \left(\frac{\Omega}{T} \right)^d$. The combination of Eq. (C5) with Eq. (C6) gives rise to

$$T \frac{\partial z}{\partial T} = -\Omega \frac{\partial z}{\partial \Omega}. \quad (\text{C7})$$

With consideration of Eqs. (C4), (C3), and (C7), we have $d\Omega/dT = \Omega/T$, yielding the isentropic condition $T/\Omega = \text{const}$ [24,45]. That is, the ratio of frequency to temperature Ω/T remains constant during the adiabatic process.

As $S = S(\Omega/T, z) = \text{const}$ with $\omega/T = \text{const}$ during the adiabatic process, we can obtain $z = \text{const}$, where there exists a relation of $z_1 = z_2$ and $z_3 = z_4$. Since the ground-state particle number $N_0 = z/(1-z)$, this means that no phase transition can occur in an adiabatic process. The correction factor $F(z)$ in Eq. (6) is kept constant and we obtain the isentropic condition as

$$\frac{\mathcal{V}_1}{\mathcal{V}_2} = \left(\frac{\mathcal{P}_h}{\mathcal{P}_l} \right)^{\frac{d}{d+1}} = \left(\frac{T_2}{T_1} \right)^d, \quad \frac{\mathcal{V}_4}{\mathcal{V}_3} = \left(\frac{\mathcal{P}_h}{\mathcal{P}_l} \right)^{\frac{d}{d+1}} = \left(\frac{T_3}{T_4} \right)^d. \quad (\text{C8})$$

Via comparing with $\mathcal{P}\mathcal{V}^\gamma = \text{const}$ for the classical adiabatic process, the adiabatic exponent for the d -dimensional Bose system is obtained: $\gamma = (d+1)/d$. Using Eqs. (10) and (C8), we then obtain Eq. (5). Since satisfying $T\mathcal{P}^{\frac{1}{\gamma}-1} = \text{const}$ in the adiabatic process, using Eq. (4), we can obtain the reduced temperature $t = \text{const}$ in the adiabatic process.

APPENDIX D: HEAT CAPACITY AT CONSTANT PRESSURE

From the comparison of Eq. (A6) with Eq. (A7), we find that the system energy can be given by $U = \mathcal{P}\mathcal{V}d$ with $\mathcal{V} = \Omega^{-d}$. The specific heat at constant pressure is then determined by $C_P = \left(\frac{\partial \mathcal{H}}{\partial T} \right)_{N,P}$, with enthalpy $\mathcal{H} = U + \mathcal{P}\mathcal{V} = (1+d)\mathcal{P}\mathcal{V}$, to arrive at

$$C_P = -d(1+d) \frac{\mathcal{P}}{\Omega^{d+1}} \left(\frac{\partial \Omega}{\partial T} \right)_{N,P}, \quad (\text{D1})$$

where

$$\left. \frac{\partial \Omega}{\partial T} \right|_{T \leq T_c^P} = -d \left[\frac{(d+1)\zeta(d+1)}{\lambda \Gamma(d)\zeta(d)} + \frac{\Omega}{T} \right] \quad (\text{D2})$$

can be obtained by using the condition $\partial \mathcal{P} / \partial T = 0$, with the pressure given by (B1). It follows that by substituting Eqs. (B1) and (B3) into Eq. (D1), the specific heat at constant pressure in the condensate phase reads

$$\left. \frac{C_P}{N} \right|_{T \leq T_c^P} = d(d+1) [\mathcal{X}_t + \zeta(d+1)] \times \frac{\mathcal{X}_t d + (d+1)\zeta(d+1)}{N [\mathcal{X}_t d / \lambda \Gamma(d)\zeta(d)]^d \mathcal{X}_t}, \quad (\text{D3})$$

where \mathcal{X}_t was defined in Eq. (B4).

Following the same method as in the case of the condensed phase, we analyze the specific heat for $T > T_c^P$. Inserting Eqs. (A3) and (A7) into the relations $\partial N / \partial T = 0$

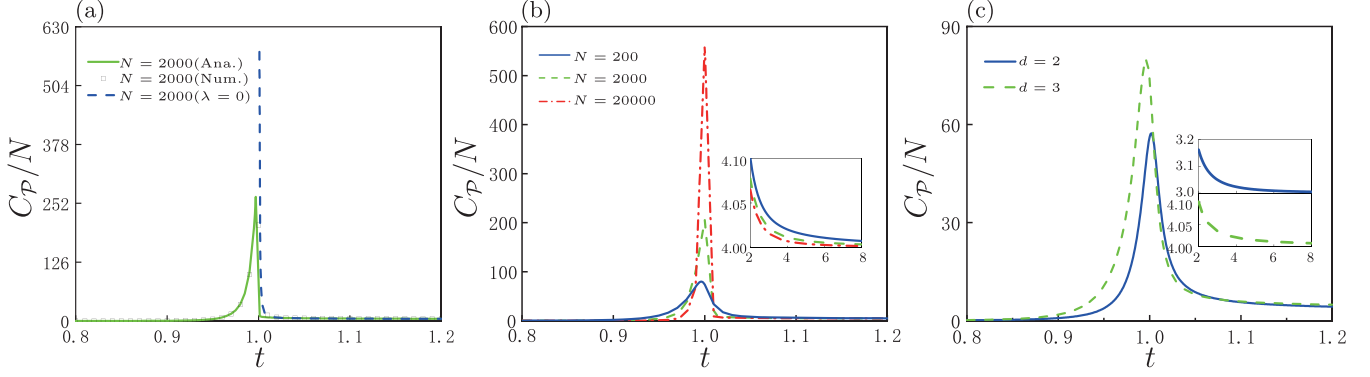


FIG. 6. The correction factor $F(z)$ as a function of the reduced temperature. (a) Numerical (black diamonds) and analytical (green solid line) solutions of the specific heat for the system with particle number $N = 2000$, comparing the calculations via setting λ in Eq. (A2) to be zero. (b) Numerical results of specific heat for particle number $N = 200, 2000, 20\,000$, and for $d = 3$. (c) Specific heat at constant pressure for particle number $N = 2000$ with $d = 2, 3$. Insets in (b) and (c): specific heat at high temperatures ($2 < t < 8$).

and $\partial P / \partial T = 0$, we have

$$\frac{\partial \Omega}{\partial T} \Big|_{T > T_c^p} = \frac{\mathcal{Y}_1 \frac{\Omega}{T} + \lambda \mathcal{A}_1 \left(\frac{\Omega}{T}\right)^2 + \lambda^2 \mathcal{C}_1 \left(\frac{\Omega}{T}\right)^3}{\mathcal{Y}_2 + \lambda \mathcal{A}_2 \frac{\Omega}{T} + \lambda^2 \mathcal{C}_2 \left(\frac{\Omega}{T}\right)^2}, \quad (\text{D4})$$

where $\mathcal{Y}_1 = d[g_d^2(z)d - (1+d)g_{d-1}(z)g_{d+1}(z)]$, $\mathcal{Y}_2 = [g_d(z)d]^2$, $\mathcal{A}_1 = d\Gamma(d-1)[(d-1)g_{d-1}(z)g_d(z) - (1+d)g_{d-2}(z)g_{d+1}(z)]$, $\mathcal{A}_2 = (1+2d)\Gamma(d)g_{d-1}(z)g_d(z)$, $\mathcal{C}_1 = \Gamma(d-1)\Gamma(d)[(d-1)g_{d-1}^2(z) - g_{d-2}(z)g_d(z)d]$, $\mathcal{C}_2 = [\Gamma(d)g_{d-1}(z)]^2 + \Gamma(d-1)\Gamma(d)g_{d-2}(z)g_d(z)$. Thus, inserting Eqs. (D4), (A7), and (B6) into the relation $C_P = -d(1+d)\frac{P}{\Omega^{d+1}}\left(\frac{\partial \Omega}{\partial T}\right)_{N,P}$, we can obtain the heat capacity at constant pressure in the noncondensed phase, given by

$$\begin{aligned} \frac{C_P}{N} \Big|_{T > T_c^p} &= -\frac{d(d^2-1)\mathcal{X}g_d(z)}{t^{d+1}[(d-1)g_d(z)^2 + g_{d-1}(z)\mathcal{X}_{t,z}d]} \\ &\times \frac{[\Gamma(d)g_d(z)]^2\mathcal{Y}_1 + d\Gamma(d)g_d(z)\mathcal{A}_1\mathcal{X}_{t,z} + \mathcal{C}_1[\mathcal{X}_{t,z}d]^2}{[\Gamma(d)g_d(z)]^2\mathcal{Y}_2 + d\Gamma(d)g_d(z)\mathcal{A}_2\mathcal{X}_{t,z} + \mathcal{C}_2[\mathcal{X}_{t,z}d]^2}, \end{aligned} \quad (\text{D5})$$

where $\mathcal{X}_{t,z} = \mathcal{X}/t^{d+1} - g_{d+1}(z)$.

In the thermodynamic limit, Eq. (D5) gives rise to

$$\begin{aligned} \frac{C_P}{N} \Big|_{T > T_c^p}^{N \rightarrow \infty} &= (d+1) \frac{g_{d+1}(z)g_{d-1}(z)}{g_d(z)^2} \\ &\times \left[(d+1) \frac{g_{d+1}(z)}{g_d(z)} - d \frac{g_d(z)}{g_{d-1}(z)} \right] \end{aligned} \quad (\text{D6})$$

which, in the high-temperature limit, gives rise to $C_P \Big|_{T > T_c^p}^{N \rightarrow \infty} = N(d+1)$, as expected.

The analytical expressions for the heat capacity, given by Eqs. (D3) and (D5), were found based on the two approximations, $z \approx 1$ for $T < T_c^p$ and $N_0 \approx 0$ for $T > T_c^p$, but they are confirmed by our exact numerical calculation, as shown in Fig. 6(a), where $N = 2000$. The nice agreement between the numerical and analytical solutions supports an argument in favor of our analytical approach. We may notice the quite

different results when ignoring the second term in Eq. (A2), as also shown in Fig. 6(a), demonstrating the significance of the finite-size correction.

Figure 6(b) shows the specific heat per particle at constant pressure as a function of reduced temperature t for the three-dimensional trapped Bose system with $N = 200, 2000$ and $20\,000$, respectively. We observed that the specific heat becomes sharper with increasing particle number N at the critical point, exhibiting a divergent behavior of the specific heat. This is because, at the critical point, the majority of the energy input is not employed to heat up but rather to make the phase transition, so a finite heat exchange is accompanied by an infinitesimal change in temperature. Figure 6(c) shows the specific heat per particle at constant pressure for the Bose system with $N = 200$ particles confined in different dimensional harmonic trap, $d = 2$ and 3 [70], respectively. Given this particle number, the specific heat at the critical point becomes larger as the dimension increases.

APPENDIX E: METHOD FOR CALCULATING THE EFFICIENCY AT MAXIMUM POWER

Here we show how to numerically determine the efficiency at maximum power by considering the three cases as in Sec. IID of the main text.

1. Case I: The noncondensation regime.

Let us consider the case for the machine cycle work at temperatures higher than the phase transition, i.e., reduced temperature $t_1 > 1$ and $t_3 > 1$ with $t_1 = T_1/T_c^p$, $t_3 = T_3/T_c^p$.

By setting $\partial P / \partial t_1 = 0$, $\partial P / \partial t_3 = 0$, and $\partial P / \partial r = 0$, where the power output P was given by Eq. (18), we have the following equations:

$$F(z_1) + t_1 \frac{\partial F(z_1)}{\partial t_1} = \frac{\mathcal{I}_1}{\mathcal{I}_3} [t_3 F(z_3) - t_1 F(z_1)], \quad (\text{E1})$$

$$F(z_3) + t_3 \frac{\partial F(z_3)}{\partial t_3} = \frac{\mathcal{I}_2}{\mathcal{I}_3} [t_3 F(z_3) - t_1 F(z_1)], \quad (\text{E2})$$

$$\frac{(1-r)(t_3 - t_1)}{(t_1 T_l - r t_1 T_h)} = \frac{\mathcal{I}_3(t_3 T_l - r t_1 T_h)}{\kappa_l r t_1 T_l T_h}, \quad (\text{E3})$$

where we have used $\mathcal{I}_1 \equiv \frac{\kappa_h}{t_1 - t_l} - \frac{\kappa_l T_l}{t_1 T_l - r t_l T_h}$, $\mathcal{I}_2 \equiv \frac{\kappa_h}{t_3 - t_l} - \frac{\kappa_l T_l}{t_3 T_l - r t_l T_h}$, and $\mathcal{I}_3 = \ln\left(\frac{t_3 - t_l}{t_1 - t_l}\right) \kappa_h + \ln\left(\frac{t_1 T_l - r t_l T_h}{t_3 T_l - r t_l T_h}\right) \kappa_l$. The factors in $\partial F(z_1)/\partial t_1$ and $\partial F(z_3)/\partial t_3$ in Eqs. (E1) and (E2) can be obtained by using Eq. (6) to arrive at

$$\begin{aligned} \frac{\partial F(z_j)}{\partial t} = & t \frac{\partial z_j}{\partial t_j} \frac{(d-1) \mathcal{X} t_j^d g_{d-1}(z_j) g_d^2(z_j) + d [g_{d-1}^2(z_j) - g_{d-2}(z_j) g_d(z_j)] \mathcal{X}_{t_j, z_j}^*}{z_j t_j [(d-1) t_j^d g_d^2(z_j) + d g_{d-1}(z_j) \mathcal{X}_{t_j, z_j}^*]^2} \\ & - \frac{(d-1) \mathcal{X} t_j^d z_j g_d(z_j) d [(d-1) g_d^2(z_j) - g_{d-1}(z_j) g_{d+1}(z_j) d]}{z_j t_j [(d-1) t_j^d g_d^2(z_j) + d g_{d-1}(z_j) \mathcal{X}_{t_j, z_j}^*]^2}, \end{aligned} \quad (\text{E4})$$

where $\mathcal{X}_{t_j, z_j}^* = \mathcal{X} - t_j^d g_{d+1}(z_j)$, with \mathcal{X} defined by Eq. (4). Substituting Eq. (B6) into Eq. (1), the total particle number for the system in the out-of-condensation regime where $N_0 \rightarrow 0$ can be reexpressed as

$$N = \left(\frac{\Gamma(d) \lambda g_d(z_j)}{d [\mathcal{X}/t_j^{d+1} - g_{d+1}(z_j)]} \right)^d g_d(z_j) + \lambda \Gamma(d-1) \left(\frac{\Gamma(d) \lambda g_d(z_j)}{d [\mathcal{X}/t_j^{d+1} - g_{d+1}(z_j)]} \right)^{d-1} g_{d-1}(z_j). \quad (\text{E5})$$

We use the condition $\partial N/\partial t_j = 0$ due to the conservation of the total particle number to obtain

$$\frac{\partial z_j}{\partial t_j} = - \frac{d(d+1) z_j \mathcal{X} \Gamma(d) g_d(z_j) [g_d^2(z_j) + g_{d-1}(z_j) \mathcal{X}_{t_j, z_j}]}{t_j^{2+d} \Gamma(d) g_d^2(z_j) [d g_d^2(z_j) + (1+d) g_{d-1}(z_j) \mathcal{X}_{t_j, z_j}] + t_j d \Gamma(d-1) \mathcal{X}_{t_j, z_j} t_j^{d+1} [(d-1) g_{d-1}(z_j) g_d^2(z_j) + \mathcal{M} \mathcal{X}_{t_j, z_j}]}, \quad (\text{E6})$$

where $\mathcal{M} = (d-1) g_{d-1}^2(z_j) + g_{d-2}(z_j) g_d(z_j)$ has been used, and \mathcal{X}_{t_j, z_j} has been defined by Eq. (D5).

Given particle number N , dimension d , and reduced temperature t_j , the fugacity z_j is numerically determined according to Eq. (E5). After having substituting Eq. (E4) [where $\partial z_j/\partial t_j$ was given by Eq. (E6)] into Eqs. (E1) and (E2), we can numerically extract values of r, t_1, t_3 by solving the system of nonlinear equations (E1), (E2), and (E3), provided that the parameters N, d, T_h, T_l , and t_l are given. As a consequence, the efficiency defined by Eq. (12) is numerically obtained under the condition of maximal power.

2. Case II: Near-critical point regime

We consider another case for the machine cycle work across the Bose-Einstein condensation and thus $t_3 > 1$ and $t_1 \leq 1$. For the expression of the power output [cf. Eq. (18)], $F(z_3)$ is still given by Eq. (6), but $F(z_1)$ with $z_1 \rightarrow 1$ becomes

$$F(z_1 = 1) = \frac{\zeta(d+1) + \mathcal{X}_{t_1}}{\zeta(d) + \frac{d}{d-1} \frac{\zeta(d-1)}{\zeta(d)} \mathcal{X}_{t_1}} \left(\frac{\Gamma(d) \lambda \zeta(d)}{\mathcal{X}_{t_1} d} \right)^{d-1} \frac{\Gamma(d) \lambda \zeta(d)^2}{\mathcal{X}_{t_1} N d} \left[\frac{\Gamma(d) \lambda \zeta(d)^2}{\mathcal{X}_{t_1} N d} + \frac{\lambda \zeta(d-1)}{N} \right], \quad (\text{E7})$$

with $\mathcal{X}_{t_1} = \mathcal{X}/t_1^{d+1} - \zeta(d+1)$. Based on the same approach as that used in the noncondensation case, we maximize the power output with respect to r, t_1, t_3 to obtain

$$F(z_1) + t_1 \frac{\partial F(z_1)}{\partial t_1} = \frac{\mathcal{I}_1}{\mathcal{I}_3} [t_3 F(z_3) - t_1 F(z_1)], \quad (\text{E8})$$

$$F(z_3) + t_3 \frac{\partial F(z_3)}{\partial t_3} = \frac{\mathcal{I}_2}{\mathcal{I}_3} [t_3 F(z_3) - t_1 F(z_1)], \quad (\text{E9})$$

$$\frac{(1-r)(t_3 - t_1)}{(t_1 T_l - r t_l T_h)} = \frac{\mathcal{I}_3 (t_3 T_l - r t_l T_h)}{\kappa_l r t_l T_l T_h}, \quad (\text{E10})$$

where $\mathcal{I}_{1,2,3}$ were defined below Eq. (E3), $\partial F(z_3)/\partial t_3$ is given by Eq. (E4), and $\partial F(z_1)/\partial t_1$ can be derived by using Eq. (E7),

$$\frac{\partial F(z_1 \rightarrow 1)}{\partial t} = \frac{\mathcal{I}_4 [d \mathcal{X}_t \zeta(d-1)]^2 [d (\mathcal{X}/t^{d+1}) - \mathcal{X}_t] + (d+1) \Gamma(d) \zeta(d)^4 [d (\mathcal{X}/t^{d+1}) - \mathcal{X}_t] + d \mathcal{X}_t \zeta(d-1) \zeta(d)^2 \mathcal{I}_5}{t N \mathcal{X}_t \Gamma(d) [d \mathcal{X}_t \zeta(d-1) + (d-1) \zeta(d)^2]^2}, \quad (\text{E11})$$

with \mathcal{X}_t defined in Eq. (6), $\mathcal{I}_4 = \mathcal{X} [\lambda \Gamma(d) \zeta(d) / (\mathcal{X}_t d)]^d (d^2 - 1)/t^{d+1}$ and $\mathcal{I}_5 = [2 - 3d + d^2 + \Gamma(d+1)] \mathcal{X}_t + \zeta(1 + d)[(d-1)^2 + (1+d)\Gamma(d)]$. We substitute Eq. (6) (with $j=3$), Eq. (E7), and Eq. (E11) into the system of Eqs. (E8),

(E9), and (E10), which, together with Eqs. (E5) and (E6), lead to the optimal values of r, t_1, t_3 under maximal power. We then obtain the efficiency, $\eta = 1 - r$, for the machine operating across the phase transition and working at maximum power.

3. Case III: The high-temperature limit

When the machine cycle operates in the high-temperature regime, i.e., $t_1 \gg 1$ and $t_3 \gg 1$, we have $F(z_1) \approx 1$ and $F(z_3) \approx 1$. In such a limit, the power output given by Eq. (18) simplifies to

$$P = \frac{N(1+d)(1-r)\kappa_h\kappa_l T_l [t_3 - t_1]}{\beta r t_l \left[\ln \left(\frac{t_3 - t_l}{t_1 - t_l} \right) \kappa_h + \ln \left(\frac{t_1 T_l - r t_l T_h}{t_3 T_l - r t_l T_h} \right) \kappa_l \right]}. \quad (\text{E12})$$

By setting $\partial P / \partial t_1 = 0$, $\partial P / \partial t_3 = 0$, and $\partial P / \partial r = 0$, we have the following equations:

$$\mathcal{I}_1(t_3 - t_1) = \mathcal{I}_3, \quad (\text{E13})$$

$$\mathcal{I}_2(t_3 - t_1) = \mathcal{I}_3, \quad (\text{E14})$$

$$\frac{(1-r)(t_3 - t_1)}{(t_1 T_l - r t_l T_h)} = \frac{\mathcal{I}_3(t_3 T_l - r t_l T_h)}{\kappa_l r t_l T_l T_h}, \quad (\text{E15})$$

where $\mathcal{I}_{1,2,3}$ were defined after Eq. (E3). A comparison between Eqs. (E13) and (E14) leads to $\mathcal{I}_1 = \mathcal{I}_2$, which means that

$$\frac{\kappa_h}{t_1 - t_l} - \frac{\kappa_l T_l}{t_1 T_l - r t_l T_h} = \frac{\kappa_h}{t_3 - t_l} - \frac{\kappa_l T_l}{t_3 T_l - r t_l T_h}. \quad (\text{E16})$$

Using Eqs. (E13) and (E15), we have

$$\frac{\kappa_h}{t_1 - t_l} - \frac{\kappa_l T_l}{t_1 T_l - r t_l T_h} = \frac{\kappa_l r t_l T_l T_h (1-r)}{(t_1 T_l - r t_l T_h)(t_3 T_l - r t_l T_h)}. \quad (\text{E17})$$

With consideration of Eqs. (E16) and (E17), we can obtain

$$r = \sqrt{T_l / T_h} \quad (\text{E18})$$

and

$$t_3 = \frac{t_l [\kappa_l (t_1 - t_l) T_l - \kappa_h t_l \sqrt{T_l T_h} + \kappa_h t_l T_h]}{\kappa_l (t_1 - t_l) T_l + \kappa_h (t_l \sqrt{T_l T_h} - t_1 T_l)}. \quad (\text{E19})$$

When $\kappa_l = \kappa_h$, Eq. (E19) becomes $t_3 = t_1 - t_l + t_l \sqrt{T_h / T_l}$, which, together with Eq. (17), gives rise to $\tau_l = \tau_h$.

We note that we have used the optimization scheme by using the extremal condition $\{\partial \mathcal{P} / \partial t_1 = 0, \partial \mathcal{P} / \partial t_3 = 0, \partial \mathcal{P} / \partial r = 0\}$ to determine the efficiency at maximum power, for the sake of mathematical simplicity when the machine works across the Bose-Einstein condensation or in the near-critical point regime. Since τ_h and τ_l are functions of t_1 and t_3 , the extremal condition we used is equivalent to that $\{\partial \mathcal{P} / \partial \tau_h = 0, \partial \mathcal{P} / \partial \tau_l = 0, \partial \mathcal{P} / \partial r = 0\}$. In the latter case, the power output $P = W / \tau_{\text{cyc}}$, with work W given by Eq. (11), should be reexpressed in terms of τ_h and τ_l ,

$$P = \frac{N(1+d)(r-1)[R_1 F(z_1) + R_2 F(z_3)]}{\beta r (\tau_l + \tau_h) [\exp(\kappa_l \tau_l) + \exp(\kappa_h \tau_h) - 1]}, \quad (\text{E20})$$

where $R_1 = \exp(\kappa_h \tau_h) [\exp(\kappa_l \tau_l) - 1] T_l + [\exp(\kappa_h \tau_h) - 1] r T_h$ and $R_2 = T_l [1 - \exp(\kappa_l \tau_l)] - \exp(\kappa_l \tau_l) [\exp(\kappa_h \tau_h) - 1] r T_h$.

As an example, we now maximize the power output with respect to r and $\tau_{l,h}$ to obtain the corresponding efficiency. In the high-temperature limit where the correction factor $F(z) \rightarrow 1$, the power output (E20) simplifies

to

$$P = 2NT_h(1+d) \left(\frac{1}{r} - 1 \right) (r + \eta_C - 1) \times \frac{\sinh(\kappa_l \tau_l / 2) \sinh(\kappa_h \tau_h / 2)}{\beta (\tau_h + \tau_l) \sinh[(\kappa_h \tau_h + \kappa_l \tau_l) / 2]}. \quad (\text{E21})$$

The power P is therefore written as a product of two terms: a term $\mathcal{F} \equiv 2NT_h(1+d)(1-r)(r + \eta_C - 1)/r$, which explicitly depends on the external parameters d , r , and $T_{h,l}$, and the other one $\mathcal{G} \equiv \frac{\sinh(\kappa_l \tau_l / 2) \sinh(\kappa_h \tau_h / 2)}{\beta (\tau_h + \tau_l) \sinh[(\kappa_h \tau_h + \kappa_l \tau_l) / 2]}$ being only dependent on the time allocations τ_h and τ_l . Given the external constraints, maximizing the power output is realized by setting $\partial \mathcal{G} / \partial \tau_h = 0$ and $\partial \mathcal{G} / \partial \tau_l = 0$, giving rise to the optimal protocol, $\kappa_h [\cosh(\kappa_l \tau_l) - 1] = \kappa_l [\cosh(\kappa_h \tau_h) - 1]$, and thus $\tau_h = \tau_l$ if $\kappa_l = \kappa_h$. In such a case, maximizing the power output by performing $\partial \mathcal{F} / \partial r = 0$, we obtain the pressure ratio as $r = \sqrt{1 - \eta_C}$, showing that the efficiency at maximum power is the same as the CA efficiency η_{CA} .

APPENDIX F: ESTIMATE: AN EXPLANATION OF WHY EFFICIENCY AT MAXIMUM POWER IS BEYOND THE UNIVERSALITY OF CA VALUE

While obtaining the exactly analytical expression of efficiency at maximum power in the near-critical point regime is a formidable task, we make an estimate of the optimal efficiency by considering the critical behavior of the heat capacity. Under the assumption that the machine cycle is in the quasistatic limit, the system temperatures T_3 and T_1 tend to be the reservoir temperatures T_h and T_l , respectively. In the regime close to the critical point, the heat capacity at constant pressure scales as $C_P / N \sim |t - 1|^{-\alpha}$, where α is the critical exponent and $t = T / T_c^P$ indicates the reduced temperature. For the machine in the near-critical point regime with $t_h > 1$ and $t_l \leq 1$, the work output given as Eq. (19) scales as $W / N \sim \left(\frac{T_h}{T_l} - \frac{T_l}{T_l} \right) \int_{t_l}^{t_h} |t - 1|^{-\alpha} dt \sim \frac{1}{1-\alpha} \left(\frac{T_h}{T_l} - \frac{T_l}{T_l} \right) [(t_h - 1)^{1-\alpha} + (1 - t_l)^{1-\alpha}]$. By setting $\partial W / \partial t_h = 0$ and $\partial W / \partial t_l = 0$, we can obtain the relation

$$\frac{t_l^2 (t_h - 1)^\alpha}{t_h^2 (1 - t_l)^\alpha} = \frac{T_l}{T_h}. \quad (\text{F1})$$

When the Bose gas is confined in a three-dimensional harmonic trap, the critical exponent $\alpha = 1$ [71], and the root of Eq. (F1) can be expressed in terms of Carnot efficiency: $(t_h / t_l)^* = 2 / (t_l + \sqrt{t_l^2 - 4(1 - \eta_C)(1 - t_l)})$.

We consider the linear response regime where the difference between the two reservoir temperatures is small, namely, $\eta_C \ll 1$. In such a case, the optimal efficiency, $\eta^* = 1 - (1 - \eta_C)(t_h / t_l)^*$, can be expanded in terms of the Carnot efficiency η_C by keeping the first order: $\eta^* = [1 - (1 - t_l)t_l]\eta_C + \mathcal{O}(\eta_C^2)$. As the machine works in the near-critical point regime, t_l is close to 1, thereby implying that the optimal efficiency may approach the Carnot efficiency.

If the system is much away from the critical point, the heat capacity per particle behaves as $C_P / N \sim 1$. Using Eq. (F1) and the relation $r = t_h T_l / (t_l T_h)$, we find that the efficiency at maximum power can be approximated by $\eta = 1 - \sqrt{T_l / T_h} = \eta_C / 2 + \eta_C^2 / 8 + \mathcal{O}(\eta_C^3)$, which is the same as the CA

efficiency. We therefore conclude that the efficiency at maximum power of the machine operating in the near-critical point regime will be much greater than the CA efficiency, due to

the singularity of the heat capacity at the near-critical point for the three-dimensional and two-dimensional [72] Bose gas.

- [1] A. Dechant, N. Kiesel, and E. Lutz, All-optical nanomechanical heat engine, *Phys. Rev. Lett.* **114**, 183602 (2015).
- [2] J. Rosnagel, S. T. Dawkins, K. N. Tolazzi, O. Abah, E. Lutz, F. Schmidt-Kaler, and K. Singer, A single-atom heat engine, *Science* **352**, 325 (2016).
- [3] P. Fadler, A. Friedenberger, and E. Lutz, Efficiency at maximum power of a carnot quantum information engine, *Phys. Rev. Lett.* **130**, 240401 (2023).
- [4] R. J. de Assis, T. M. de Mendonca, C. J. Villas-Boas, A. M. de Souza, R. S. Sarthour, I. S. Oliveira, and N. G. de Almeida, Efficiency of a quantum otto heat engine operating under a reservoir at effective negative temperatures, *Phys. Rev. Lett.* **122**, 240602 (2019).
- [5] J. P. S. Peterson, T. B. Batalhão, M. Herrera, A. M. Souza, R. S. Sarthour, I. S. Oliveira, and R. M. Serra, Experimental characterization of a spin quantum heat engine, *Phys. Rev. Lett.* **123**, 240601 (2019).
- [6] J. Klaers, S. Faelt, A. Imamoglu, and E. Togan, Squeezed thermal reservoirs as a resource for a nanomechanical engine beyond the carnot limit, *Phys. Rev. X* **7**, 031044 (2017).
- [7] F. Altintas, A. Ü. C. Hardal, and Ö. E. Müstecaplıoğlu, Rabi model as a quantum coherent heat engine: From quantum biology to superconducting circuits, *Phys. Rev. A* **91**, 023816 (2015).
- [8] C. L. Latune, G. Pleasance, and F. Petruccione, Cyclic quantum engines enhanced by strong bath coupling, *Phys. Rev. Appl.* **20**, 024038 (2023).
- [9] J. Lu, Z. Wang, J. Peng, C. Wang, J.-H. Jiang, and J. Ren, Geometric thermodynamic uncertainty relation in a periodically driven thermoelectric heat engine, *Phys. Rev. B* **105**, 115428 (2022).
- [10] M. Boubakour, T. Fogarty, and T. Busch, Interaction-enhanced quantum heat engine, *Phys. Rev. Res.* **5**, 013088 (2023).
- [11] V. F. Lisboa, P. R. Dieguez, J. R. Guimarães, J. F. G. Santos, and R. M. Serra, Experimental investigation of a quantum heat engine powered by generalized measurements, *Phys. Rev. A* **106**, 022436 (2022).
- [12] J.-T. Bu, J.-Q. Zhang, G.-Y. Ding, J.-C. Li, J.-W. Zhang, B. Wang, W.-Q. Ding, W.-F. Yuan, L. Chen, S. K. Özdemir, F. Zhou, H. Jing, and M. Feng, Enhancement of quantum heat engine by encircling a liouvillian exceptional point, *Phys. Rev. Lett.* **130**, 110402 (2023).
- [13] M. L. Bera, S. Juliá-Farré, M. Lewenstein, and M. N. Bera, Quantum heat engines with Carnot efficiency at maximum power, *Phys. Rev. Res.* **4**, 013157 (2022).
- [14] R. Dann and R. Kosloff, Quantum signatures in the quantum Carnot cycle, *New J. Phys.* **22**, 013055 (2020).
- [15] Q. Bouton, J. Nettersheim, S. Burgardt, D. Adam, E. Lutz, and A. Widera, A quantum heat engine driven by atomic collisions, *Nat. Commun.* **12**, 2063 (2021).
- [16] J. W. Deng, Q.-H. Wang, Z. H. Liu, P. Hänggi, and J. B. Gong, Boosting work characteristics and overall heat-engine performance via shortcuts to adiabaticity: Quantum and classical systems, *Phys. Rev. E* **88**, 062122 (2013).
- [17] M. Campisi and R. Fazio, The power of a critical heat engine, *Nat. Commun.* **7**, 11895 (2016).
- [18] J. Klatzow, J. N. Becker, P. M. Ledingham, C. Weinzetl, K. T. Kaczmarek, D. J. Saunders, J. Nunn, I. A. Walmsley, R. Uzdin, and E. Poem, Experimental demonstration of quantum effects in the operation of microscopic heat engines, *Phys. Rev. Lett.* **122**, 110601 (2019).
- [19] X. L. Huang, L. C. Wang, and X. X. Yi, Quantum Brayton cycle with coupled systems as working substance, *Phys. Rev. E* **87**, 012144 (2013).
- [20] H. Wang and G. X. Wu, Optimization criteria of a Bose Brayton heat engine, *Chin. Phys. B* **21**, 010505 (2012).
- [21] H. Saygin and A. Şişman, Brayton refrigeration cycles working under quantum degeneracy conditions, *Appl. Energy* **69**, 77 (2001).
- [22] S. Hamedani Raja, S. Maniscalco, G. S. Paroanu, J. P. Pekola, and N. L. Gullo, Finite-time quantum Stirling heat engine, *New J. Phys.* **23**, 033034 (2021).
- [23] G. Thomas, D. Das, and S. Ghosh, Quantum heat engine based on level degeneracy, *Phys. Rev. E* **100**, 012123 (2019).
- [24] N. M. Myers, F. J. Peña, O. Negrete, P. Vargas, G. D. Chiara, and S. Deffner, Boosting engine performance with Bose-Einstein condensation, *New J. Phys.* **24**, 025001 (2022).
- [25] J. Li, T. Fogarty, S. Campbell, X. Chen, and T. Busch, An efficient nonlinear Feshbach engine, *New J. Phys.* **20**, 015005 (2018).
- [26] Y. H. Ma, S. H. Su, and C. P. Sun, Quantum thermodynamic cycle with quantum phase transition, *Phys. Rev. E* **96**, 022143 (2017).
- [27] M. Gluza, J. Sabino, N. H. Y. Ng, G. Vitagliano, M. Pezzutto, Y. Omar, I. Mazets, M. Huber, J. Schmiedmayer, and J. Eisert, Quantum field thermal machines, *PRX Quantum* **2**, 030310 (2021).
- [28] N. Y. Halpern, C. D. White, S. Gopalakrishnan, and G. Refael, Quantum engine based on many-body localization, *Phys. Rev. B* **99**, 024203 (2019).
- [29] T. Fogarty and T. Busch, A many-body heat engine at criticality, *Quantum Sci. Technol.* **6**, 015003 (2021).
- [30] J. Jaramillo, M. Beau, and A. del Campo, Quantum supremacy of many-particle thermal machines, *New J. Phys.* **18**, 075019 (2016).
- [31] G. A. Barrios, F. Albarrán-Arriagada, F. A. Cárdenas-López, G. Romero, and J. C. Retamal, Role of quantum correlations in light-matter quantum heat engines, *Phys. Rev. A* **96**, 052119 (2017).
- [32] F. Altintas, A. Ü. C. Hardal, and Ö. E. Müstecaplıoğlu, Quantum correlated heat engine with spin squeezing, *Phys. Rev. E* **90**, 032102 (2014).
- [33] Y. Xiao, D. H. Liu, J. Z. He, Y. L. Ma, Z. Q. Wu, and J. H. Wang, Quantum Otto engine with quantum correlations, *Phys. Rev. A* **108**, 042614 (2023).

- [34] J. Koch, K. Menon, E. Cuestas, S. Barbosa, E. Lutz, T. Fogarty, T. Busch, and A. Widera, A quantum engine in the BEC-BCS crossover, *Nature (London)* **621**, 723 (2023).
- [35] J. Lee and H. E. Stanley, Phase transition in the multifractal spectrum of diffusion-limited aggregation, *Phys. Rev. Lett.* **61**, 2945 (1988).
- [36] W. F. Brinkman and S. Engelsberg, Spin-fluctuation contributions to the specific heat, *Phys. Rev.* **169**, 417 (1968).
- [37] A. N. Chaba and R. K. Pathria, Bose-Einstein condensation in a two-dimensional system at constant pressure, *Phys. Rev. B* **12**, 3697 (1975).
- [38] M. H. Anderson, J. R. Ensher, M. R. Matthews, C. E. Wieman, and E. A. Cornell, Observation of Bose-Einstein condensation in a dilute atomic vapor, *Science* **269**, 198 (1995).
- [39] M. W. Zwierlein, C. A. Stan, C. H. Schunck, S. M. F. Raupach, S. Gupta, Z. Hadzibabic, and W. Ketterle, Observation of Bose-Einstein condensation of molecules, *Phys. Rev. Lett.* **91**, 250401 (2003).
- [40] W. Ketterle and N. J. van Druten, Bose-Einstein condensation of a finite number of particles trapped in one or three dimensions, *Phys. Rev. A* **54**, 656 (1996).
- [41] M. Z. Li, L. X. Chen, J. C. Chen, Z. J. Yan, and C. H. Chen, Bose-Einstein condensation of a finite number of particles trapped in any-dimensional space, *Phys. Rev. A* **60**, 4168 (1999).
- [42] C. T. Tan, Q. Wang, X. R. Du, Y. L. Ma, Dimensional crossover of Bose-Einstein condensation of atomic gases in anisotropic harmonic traps, *Ann. Phys.* **440**, 168843 (2022).
- [43] S. Grossmann and M. Holthaus, λ -Transition to the Bose-Einstein Condensate, *Z. Naturforsch. A* **50**, 921 (1995).
- [44] H. Haugerud, T. Haugset, and F. Ravndal, A more accurate analysis of Bose-Einstein condensation in harmonic traps, *Phys. Lett. A* **225**, 18 (1997).
- [45] S. Deffner, Efficiency of harmonic quantum Otto engines at maximal power, *Entropy* **20**, 875 (2018).
- [46] J. F. Chen, C. P. Sun, and H. Dong, Achieve higher efficiency at maximum power with finite-time quantum Otto cycle, *Phys. Rev. E* **100**, 062140 (2019).
- [47] J.-H. Park and S.-W. Kim, Thermodynamic instability and first-order phase transition in an ideal Bose gas, *Phys. Rev. A* **81**, 063636 (2010).
- [48] G. A. Baker and J. W. Essam, Effects of Lattice Compressibility on Critical Behavior, *Phys. Rev. Lett.* **24**, 447 (1970).
- [49] J. Chen and B. Lin, Low-temperature behaviour of an ideal Bose gas and some forbidden thermodynamic cycles, *J. Phys. A: Math. Gen.* **36**, 11385 (2003).
- [50] F. L. Curzon and B. Ahlborn, Efficiency of a Carnot engine at maximum power output, *Am. J. Phys.* **43**, 22 (1975).
- [51] C. de Tomás, A. Calvo Hernández, and J. M. M. Roco, Optimal low symmetric dissipation Carnot engines and refrigerators, *Phys. Rev. E* **85**, 010104(R) (2012).
- [52] Z. C. Tu, Recent advance on the efficiency at maximum power of heat engines, *Chin. Phys. B* **21**, 020513 (2012).
- [53] M. Esposito, R. Kawai, K. Lindenberg, and C. Van den Broeck, Efficiency at maximum power of low-dissipation carnot engines, *Phys. Rev. Lett.* **105**, 150603 (2010).
- [54] T. Schmiedl and U. Seifert, Efficiency at maximum power: An analytically solvable model for stochastic heat engines, *Europhys. Lett.* **81**, 20003 (2008).
- [55] M. Esposito, K. Lindenberg, and C. Van den Broeck, Universality of efficiency at maximum power, *Phys. Rev. Lett.* **102**, 130602 (2009).
- [56] S. Sheng and Z. C. Tu, Constitutive relation for nonlinear response and universality of efficiency at maximum power for tight-coupling heat engines, *Phys. Rev. E* **91**, 022136 (2015).
- [57] Q. Liu, J. Z. He, Y. L. Ma, and J. H. Wang, Finite-power performance of quantum heat engines in linear response, *Phys. Rev. E* **100**, 012105 (2019).
- [58] M. V. S. Bonança, Approaching Carnot efficiency at maximum power in linear response regime, *J. Stat. Mech.* (2019) 123203.
- [59] Z. Yan and J. Chen, A generalized Rutgers formula derived from the theory of endoreversible cycles, *Phys. Lett. A* **217**, 137 (1996).
- [60] T. Yilmaz, A new performance criterion for heat engines: Efficient power, *J. Energy Inst.* **79**, 38 (2006).
- [61] L. Chen, Z. Ding, J. Zhou, W. Wang, and F. Sun, Thermodynamic performance optimization for an irreversible vacuum thermionic generator, *Eur. Phys. J. Plus* **132**, 293 (2017).
- [62] V. Romero-Rochcín, Equation of state of an interacting Bose gas confined by a harmonic trap: The role of the harmonic pressure, *Phys. Rev. Lett.* **94**, 130601 (2005).
- [63] For the two-dimensional systems with $d = 2$, the approximate $z \approx 1$ for calculating the critical temperature would lead to the unphysical divergence $\zeta(1) \rightarrow \infty$ in Eq. (A8). To avoid this low-dimensional divergence [40], we make the modification of expressions of the thermodynamic quantities by setting the zero-point energy $\varepsilon_0 = (\omega_1 + \omega_2)/2$ as the lower limit of the integral. For example, the total particle number $N = N_0 + \int_{\varepsilon_0}^{\infty} \rho(E)n(E)dE$ can be expressed as
- $$N = N_0 + \left(\frac{T}{\Omega}\right)^2 g_2(ze^{-\varepsilon_0/T}) + \lambda \frac{T}{\Omega} g_1(ze^{-\varepsilon_0/T}).$$
- [64] R. K. Pathria, *Statistical Mechanics* (Butterworth-Heinemann, Washington, DC, 1996).
- [65] J. H. Wang, Y. L. Ma, and J. Z. He, Quantum-mechanical engines working with an ideal gas with a finite number of particles confined in a power-law trap, *Europhys. Lett.* **111**, 20006 (2015).
- [66] H. T. Quan, Quantum thermodynamic cycles and quantum heat engines. II., *Phys. Rev. E* **79**, 041129 (2009).
- [67] P. Perrot, *A to Z of Thermodynamics* (Oxford University Press, New York, 1998).
- [68] H. B. Callen, *Thermodynamics and an Introduction to Thermostatistics*, 2nd ed. (Wiley, New York, 1985).
- [69] C. Wu, L. Chen, and J. Chen, *Advances in Finite-Time Thermodynamics: Analysis and Optimization* (Nova Science, New York, 2004).
- [70] Although the ground state is populated when the temperature is lower than a critical temperature, the specific heat does not show a cusp (or singularity in the thermodynamic limit) at the critical point [40]. Our calculations for the work produced by the machine in the one-dimensional case, which are not plotted in the figure, show that the onset of condensation leads to no enhancement of the work. We therefore do not consider the case when the machine works with a one-dimensional Bose gas throughout the paper.

- [71] F. Adli, H. Mohammadzadeh, M. N. Najafi, and Z. Ebadi, Condensation of nonextensive ideal Bose gas and critical exponents, *Physica A* **521**, 773 (2019).
- [72] M. I. Morales-Amador, V. Romero-Rochin, and R. Paredes, Critical exponents and fluctuations at BEC in a 2D harmonically trapped ideal gas, [arXiv:2308.02744](https://arxiv.org/abs/2308.02744).
- [73] The relation $T\mathcal{P}^{\frac{1}{\gamma}-1} = \text{const}$ during two adiabatic strokes leads to $T_{4,1} = rT_{3,2}$. In the extremal case when $r = T_l/T_h$, we then obtain $T_1 = T_l$ and $T_3 = T_h$ by substituting the relations $T_4 = T_l T_3/T_h$ and $T_2 = T_h T_1/T_l$ into Eqs. (14) and (15), leading to $t_1 = t_l$ and $t_3 = t_h$. The amounts of heat exchanged during the two isobaric strokes [given as in Eq. (9)] tend to be zero, resulting in zero work. This can also be observed in Fig. 3 for the special case when the cycle is quasistatic.
- [74] V. Singh and R. S. Johal, Low-dissipation Carnot-like heat engines at maximum efficient power, *Phys. Rev. E* **98**, 062132 (2018).
- [75] K. B. Davis, M.-O. Mewes, M. R. Andrews, N. J. Van Druten, D. S. Durfee, D. M. Kurn, and W. Ketterle, Bose-Einstein condensation in a gas of sodium atoms, *Phys. Rev. Lett.* **75**, 3969 (1995).
- [76] C. C. Bradley, C. A. Sackett, and R. G. Hulet, Bose-Einstein condensation of lithium: observation of limited condensate number, *Phys. Rev. Lett.* **78**, 985 (1997).
- [77] R. Kosloff, Quantum thermodynamics: A dynamical viewpoint, *Entropy* **15**, 2100 (2013).
- [78] G. Barontini and M. Paternostro, Ultra-cold single-atom quantum heat engines, *New J. Phys.* **21**, 063019 (2019).